

1 **Drivers of Phytoplankton Bloom Interannual Variability in the Amundsen and Pine
2 Island Polynyas**

3

4 **Guillaume Liniger^{1,2*}, Delphine Lannuzel^{1,3,4}, Sébastien Moreau^{5,6}, Michael S. Dinniman⁷,
5 Peter G. Strutton^{1,3}**

6 ¹ Institute for Marine and Antarctic Studies, University of Tasmania, Hobart, Australia

7 ² Monterey Bay Aquarium Research Institute, Moss Landing, CA, USA

8 ³ Australian Centre for Excellence in Antarctic Science, University of Tasmania, Hobart,
9 Australia

10 ⁴ Australian Antarctic Program Partnership, University of Tasmania, Hobart, Australia

11 ⁵ Norwegian Polar Institute, Tromsø, Norway

12 ⁶ iC3: Centre for ice, Cryosphere, Carbon and Climate, Department of Geosciences, UiT The
13 Arctic University of Norway, 9037 Tromsø, Norway

14 ⁷ Center for Coastal Physical Oceanography, Old Dominion University, Norfolk, VA, USA

15

16 * Corresponding Author: Guillaume Liniger (liniger@mbari.org)

17

18 **Abstract**

19 The Amundsen Sea Embayment (ASE) experiences both the highest ice shelf melt rates and the
20 highest biological productivity in West Antarctica. Using 19 years of satellite data and modelling
21 output, we investigate the long-term influence of environmental factors on the phytoplankton
22 bloom in the Amundsen Sea (ASP) and Pine Island ([PIP](#)) polynyas. We test the prevailing
23 hypothesis that changes in ice shelf melt rate could drive interannual variability in the polynyas'
24 surface chlorophyll-*a* (chl*a*) and Net Primary Productivity (NPP). We find that the interannual
25 variability and long-term change in glacial meltwater may play an important role in chl*a* variance
26 in the ASP, but not for NPP. Glacial meltwater does not explain the variability in [neither chl*a* or](#)
27 NPP in the PIP, where light and temperature are the main drivers. We attribute this to potentially
28 greater amount of iron-enriched meltwater brought to the surface by the meltwater pump

Deleted: ([PIP](#)).

Deleted: both

Deleted: and

32 downstream of the PIP, and the coastal ocean circulation accumulating and transporting iron
33 towards the ASP.

34

35 **Short Summary**

36 We investigate the phytoplankton bloom variability and its drivers in the Amundsen polynyas
37 (areas of open water within sea ice). Between 1998 and 2017, we find that changes in melting ice
38 shelves may have different impacts on biological productivity between the Amundsen Sea (ASP)
39 and Pine Island (PIP) polynyas. While ice shelves melting seems to play an important role for
40 phytoplankton growth variability in the ASP, light and warmer waters appear to be more
41 important in the PIP.

42

43 **1. Introduction**

44

45 Coastal polynyas are open ocean areas formed by strong katabatic winds pushing sea ice offshore
46 (Morales Maqueda, 2004). They are the most biologically productive areas in the Southern
47 Ocean (SO) relative to their size (Arrigo et al., 1998). This high biological productivity contrasts
48 sharply with the rest of the SO, where low iron and light availability generally co-limit
49 phytoplankton growth (Boyd et al., 2007). In West Antarctica, the Amundsen Sea Embayment
50 (ASE) hosts two of the most productive Antarctic polynyas: The Pine Island Polynya (PIP) and
51 Amundsen Sea Polynya (ASP) (Arrigo and van Dijken, 2003).

52

53 The phytoplankton community in the ASE is generally dominated by *Phaeocystis antarctica*
54 (Lee et al., 2017; Yager et al., 2016), which is adapted to low iron availability and variable light
55 conditions, and forms large summer blooms (Alderkamp et al., 2012; Yager et al., 2016).

56 Diatoms like *Fragilariopsis sp.* and *Chaetoceros sp.* are also present, often becoming more
57 important near the sea-ice edge or under shallow, stratified mixed layers where silicic acid (Si)
58 and iron (Fe) are more available (Mills et al., 2012). In exceptional years, such as 2020, diatoms
59 like *Dactyliosolen tenuijunctus* replaced *P. antarctica* as the dominant taxon, driven by
60 anomalously shallow mixed layers and sufficient Fe–Si supply (Lee et al., 2022). This dynamic
61 balance highlights how light, nutrient supply, and stratification control community composition
62 in these highly productive and complex Antarctic systems.

Formatted: Font color: Text 1

Deleted:

Formatted: Font color: Text 1

The ASE is also the Antarctic region experiencing the highest mass loss from the Antarctic ice sheet. It has been undergoing increased calving, melting, thinning and retreat over the past three decades (Paolo et al., 2015; Rignot et al., 2013; Rignot et al., 2019; Shepherd et al., 2018). In the ASE, this ice loss is mainly through enhanced basal melting of the ice shelves. This is attributed to an increase in wind-driven Circumpolar Deep Water (CDW) fluxes and ocean heat content intruding onto the continental shelf through deep troughs such as the Pine Island and Dotson-Getz, and flowing into the ice shelves cavities (Dotto et al., 2019; Jacobs et al., 2011; Pritchard et al., 2012). There, warm waters fuel intense basal melt of the Pine Island, Thwaites, and Getz ice shelves, and returns as a fresher, colder outflow that can strengthen stratification (Jenkins et al., 2010; Ha et al., 2014). The PIP and ASP differ in their exposure to CDW and in local circulation: the ASP is more strongly influenced by upwelled modified CDW (mCDW) and glacial meltwater inputs, whereas in the PIP, the deep mCDW retains more of its original offshore characteristics, with vertical exchange only significantly occurring beneath the ice shelves, leading to a more stratified and less directly ventilated surface layer (Assmann et al., 2013; Dutrieux et al., 2014). These hydrographic contrasts can shape the timing and magnitude of phytoplankton blooms and nutrient dynamics across the two polynyas.

Melting ice shelves can explain about 60% of the biomass variance between all Antarctic polynyas, suggesting that they are the primary supplier of dissolved iron (dFe) to coastal polynyas (Arrigo et al., 2015), and can directly or indirectly contribute to regional marine productivity (Bhatia et al., 2013; Gerringa et al., 2012; Hawkings et al., 2014; Herraiz-Borreguero et al., 2016). The strong melting of the ice shelves can release significant quantities of freshwater at depth (Biddle et al., 2017), resulting in a strong overturning within the ice shelves cavity, called the meltwater pump (St-Laurent et al., 2017). Modelling efforts have identified both resuspended Fe-enriched sediments and CDW entrained to the surface by the meltwater pump as the two primary sources of dFe to coastal polynyas, providing up to 31% of the total dFe, compared to 6% for direct ice shelves input (Dinniman et al., 2020; St-Laurent et al., 2017). Other drivers such as sea-ice coverage (and associated increases in light and dFe availability when sea ice retreats), or winds have also been shown to impact primary productivity in polynyas (Park et al., 2019; Park et al., 2017; Vaillancourt et al., 2003).

Formatted: Font color: Text 1

Deleted: intrusions primarily occur

Formatted: Font color: Text 1

96
97 The key question of how glacial meltwater variability may impact biological productivity in the
98 ASE has previously been raised during the ASPIRE program (Yager et al., 2012). During the
99 expedition, a significant supply of melt-laden iron-enriched seawater to the central euphotic zone
100 of the ASP was observed, potentially explaining why this area is the most biologically
101 productive in Antarctica (Randall-Goodwin et al., 2015; Sherrell et al., 2015). Other studies in
102 the Western Antarctic Peninsula and East Antarctica showed that the meltwater pump process
103 was also responsible for natural Fe supply to the surface, increasing primary productivity (Cape
104 et al., 2019; Tamura et al., 2023).

105

106 In this study, we investigate the long-term relationship between the main environmental factors
107 of the ASE and the surface biological productivity, with a focus on ice shelves melting. A
108 demonstrated relationship between glacial meltwater and phytoplankton growth would have far-
109 reaching consequences for regional productivity in coastal Antarctica, and possibly offshore,
110 over the coming decades under expected climate change scenarios (Meredith et al., 2019). We
111 test the hypothesis that changes in glacial meltwater are linked to the surface ocean primary
112 productivity variability observed over the last two decades. We use a combination of satellite
113 (ocean color and ice shelf melting rate), climate re-analysis, and model data spanning 1998 to
114 2017.

115

116 2. Material and Methods

117

118 2.1 Study area and polynya mapping

119

120 We focus on the PIP and ASP in the ASE in West Antarctica (Fig. 1). The ASE is comprised of
121 several ice shelves and glaciers, including: Abbot (Abb), Cosgrove (Cs), Pine Island (PIG),
122 Thwaites (Tw), Crosson (Cr), Dotson (Dt) and Getz (Gt). The PIG and Thwaites have received
123 significant attention in recent years due to their potentially large contribution to sea level rise
124 (Rignot et al., 2019; Scambos et al., 2017). Along with the Crosson and Dotson ice shelves, the
125 PIG and Thwaites are undergoing the highest melt rate, which is expected to increase under
126 climate change scenarios (Naughten et al., 2023; Paolo et al., 2023). The polynyas' boundaries

Formatted: Font color: Text 1

Deleted: 2022

Formatted: Font color: Text 1

Deleted: Cs

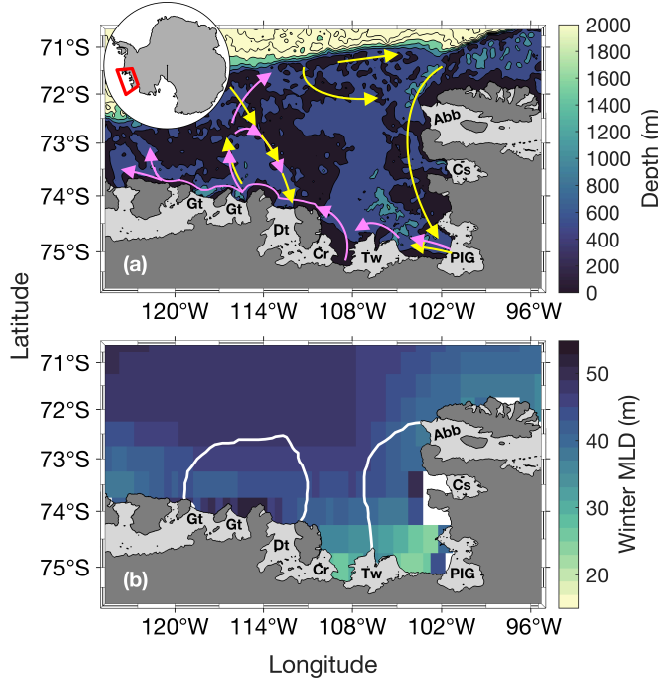
Formatted: Font color: Text 1

Deleted: The mean mixed-layer depth (MLD) in the ASP is deeper (Fig. 1b), indicating that it may better entrain deeper sources of nutrients into the upper waters.

Formatted: Font color: Text 1

Formatted: Font color: Text 1

132 were determined using a 15% sea-ice concentration (SIC) mask (Moreau et al., 2015;
133 Stammerjohn et al., 2008) for every 8-day period from June 1998 to June 2017 to accurately
134 represent the size of the polynyas through time.



154 **Fig. 1.** Study area. Panel (a) shows the bathymetry (from ETOPO1; Amante & Eakins, 2009) and
155 panel (b) shows the climatological April-September (that we call winter) mixed-layer depth
156 (MLD) from 1998 to 2016 (n=114). Panel (a) shows a simplified schematic of the local deep
157 ocean circulation (~ below 400m, yellow arrows) and upper glacial
158 meltwater/sediments/circumpolar deep water sourced dFe pathways (magenta arrows), which
159 follows the local upper ocean circulation. Schematic adapted from St-Laurent et al. (2017). The
160 white lines in panel (b) represent the climatological summer polynyas' boundaries for the
161 Amundsen (ASP; left) and Pine Island (PIP; right) polynyas. The dark grey area is mainland

Formatted: Font color: Text 1

Formatted: Font color: Text 1

Deleted: <object>

Figure...

Deleted: 1a

Formatted: Font color: Text 1

Deleted: 1b

Deleted: summer

Deleted: 2017.

Deleted: 1a

Formatted: Font color: Text 1

Deleted: Sea polnya (

Deleted: polnya (

Deleted:).

190 Antarctica. Light grey areas indicate floating ice shelves and glaciers: Abbot (Abb), Cosgrove
191 (Cs), Pine Island Glacier (PIG), Thwaites (Tw), Crosson (Cr), Dotson (Dt) and Getz (Gt).

192

193 2.2 Satellite ocean surface chlorophyll-*a* and net primary productivity

194

195 We obtained level-3 satellite surface chlorophyll-*a* concentration (*chl**a*) with spatial and
196 temporal resolution of 0.04° and 8 days from the European Space Agency (ESA) Globcolor
197 project. We used the CHL1-GSM (Garver-Siegel-Maritorena) (Maritorena and Siegel, 2005)
198 standard Case 1 water merged products consisting of the Sea-viewing Wide Field-of-view
199 (SeaWiFS), Medium Resolution Imaging Spectrometer (MERIS), Moderate Resolution Imaging
200 Spectroradiometer (MODIS-A) and Visible Infrared Imaging Suite sensors (VIIRS). We chose to
201 perform our analysis with the merged GlobColour product, which has been widely applied and
202 tested in Southern Ocean and coastal Antarctic studies (Ardyna et al., 2017; Sari El Dine et al.,
203 2025; Golder & Antoine, 2025; Nunes, Fereira & Brito, 2025), to increase our spatial and
204 temporal coverage.

205

206 We estimated phytoplankton bloom phenology metrics following the Kauko et al. (2021)
207 method. Firstly, for a given 8-day period, we applied a spatial 3x3 pixels median filter to reduce
208 gaps in missing data. Then, if a pixel was still empty, we applied the average *chl**a* of the previous
209 and following week to fill the data gap. Data were smoothed using a 4-point moving median
210 (representing a month of data). For each pixel, the threshold for the bloom detection was based
211 on 1.05 times the annual median. The threshold method is frequently used (Racault et al., 2012;
212 Siegel et al., 2002) and proven reliable at higher latitudes (Marchese et al., 2017; Soppa et al.,
213 2016; Thomalla et al., 2023). We then determined 5 main bloom metrics. The bloom start (BS) is
214 defined as the day where *chl**a* first exceeds the threshold for at least 2 consecutive 8-day periods.
215 Conversely, the bloom end is the day where *chl**a* first falls below the threshold for at least 2
216 consecutive 8-day periods. The bloom duration (BD) is the time elapsed between bloom start and
217 bloom end. The bloom mean *chl**a* (BM) and bloom maximum *chl**a* are respectively the average
218 and maximum *chl**a* value calculated during the bloom. Each year is centered around austral
219 summer, from June 10th year *n* (day 1) to June 9th year *n+1* (day 365 or 366). We also averaged
220 our 8-day data to monthly data to perform a spatial correlation analysis (see section 2.6).

Deleted: (*chl**a*)

Formatted: Font color: Text 1

Deleted: max

Formatted: Font color: Text 1

223

224 We note that satellite ocean-colour chla algorithms (including the GlobColour merged product
225 used here) are globally tuned and may underperform in optically complex waters (e.g., with
226 elevated dissolved organic matter or suspended sediments, ‘Case 2’). In the ASP, past work
227 (Park et al. 2017) showed that satellite chla climatologies reflect broad seasonal patterns that are
228 consistent with *in situ* measurements of phytoplankton biomass and photophysiology, but there is
229 limited data from regions immediately adjacent to glacier fronts or during times of strong
230 meltwater input. Thus, while we consider satellite chla to be useful for capturing spatial and
231 temporal variability at polynya scale, uncertainty likely increases in optically complex zones
232 near glacier margins or during low-light periods, and needs to be considered while interpreting
233 results.

234

235 Eight-day satellite derived Net Primary Productivity (NPP) data with 1/12° spatial resolution,
236 spanning 1998 - 2017 using the Vertically Generalized Production Model (Behrenfeld and
237 Falkowski, 1997) were obtained from the Oregon State University website. The VGPM model is
238 a chlorophyll-based approach and relies on the assumption that NPP is a function of chla,
239 influenced by light availability and maximum daily net primary production within the euphotic
240 zone. SeaWiFS-based NPP data span 1998 - 2009, MODIS-based data span 2002 - 2017. To
241 increase spatial and temporal coverage, we averaged SeaWiFS and MODIS from 2002 to 2009,
242 where there was valid data for both in a pixel. NPP data were also monthly averaged and used to
243 compare with chla spatial and temporal patterns.

244

245 We caution that our study focuses on surface productivity, and satellites cannot detect under-ice
246 phytoplankton, sea-ice algal blooms, or deeper productivity, therefore likely underestimating
247 total primary productivity (Ardyna et al., 2020; Boles et al., 2020; Douglas et al., 2024; McClish
248 & Bushinsky, 2023; Stoer & Fennel 2024).

249

250 2.3 Ice shelves volume flux

251

252 We used the latest ice shelf basal melt rate estimates from Paolo et al (2023). These estimates are
253 derived from satellite radar altimetry measurements of ice shelves height, and produced on a 3

Formatted: Font color: Text 1

Deleted: e.g.,

Deleted: shows

Deleted: chlorophyll

Formatted: Font color: Text 1

Deleted: and

Formatted: Font color: Text 1

258 km grid every 3 months, with an effective resolution of ~5 km. For this study, our basal melt
259 record spans June 1998 to June 2017. We calculated ice shelves volume flux rate for every
260 gridded cell by multiplying the basal melt rate by the cell area. Data were summed for each ice
261 shelf for a 3-month period. A 5-point (15 months) running mean was applied to reduce noise,
262 such as spurious effects induced by seasonality on radar measurements over icy surfaces (Paolo
263 et al., 2016), and data were temporally averaged from October to March to match the SO
264 phytoplankton growth season (Arrigo et al., 2015), providing yearly mean values. The Abbot,
265 Cosgrove, Thwaites, PIG, Crosson, Dotson and Getz ice shelves were used to calculate a single
266 total meltwater volume flux (TVFall) for the ASE to investigate the link with surface chla and
267 NPP. We also investigated the relationship between each polynyas' productivity and their closest
268 ice shelf. The Abbot, Cosgrove, PIG and Thwaites ice shelves were used to calculate the flux
269 rate in the PIP (TVFpip) while the Thwaites, Crosson, Dotson and Getz ice shelves were chosen
270 for the ASP (TVFasp). The Thwaites was used in both due to its central position between the two
271 polynyas. We thereafter use the term glacial meltwater which defines meltwater resulting from
272 ice shelf melting.

273

274 2.4 Simulated dFe distribution

275

276 The spatial distribution of dFe from different sources in the embayment was investigated from
277 Dinniman et al. (2020) model output. The model used is a Regional Ocean Modelling System
278 (ROMS) model, with a 5 km horizontal resolution and 32 terrain following vertical layers and
279 includes sea-ice dynamics, as well as mechanical and thermodynamic interaction between ice
280 shelves and the ocean. The model time run spans seven years and simulates fourteen different
281 tracers to understand dFe supply across the entire Antarctic coastal zone, with the last two years
282 simulating biological uptake. For the purpose of this study, we only use four different dFe
283 sources/tracers in the ASE: ice shelf melt, CDW, sediments and sea ice. Each tracer estimation is
284 independent from each other, meaning that one source does not affect the other, and they have
285 the same probability for biological uptake by phytoplankton. That is, dFe from all sources can
286 equally be taken up by phytoplankton. This is parametrized in the model as all iron molecules
287 being bound to a ligand and therefore remaining in solution in a bioavailable form (Gledhill &
288 Buck, 2012). For a detailed and complete explanation of the model, see Dinniman et al. (2020).

Formatted: Font color: Text 1

Deleted: Pine Island Glacier

Formatted: Font color: Text 1

290

291 2.5 Other environmental parameters

292

293 We used SIC data spanning June 1998 to June 2017 from the National Snow and Ice Data Center
294 (Cavalieri et al., 1996). The data are Nimbus-7 SMMR and SSMI/SSMIS passive microwave
295 daily SIC with 25 km spatial resolution. We computed the sea-ice retreat time (IRT) and open
296 water period (OWP) metrics using a 15% threshold (Stammerjohn et al., 2008). Daily data were
297 monthly averaged to perform a spatial correlation analysis (see section 2.6).

298

299 We collected monthly level-4 Optimum Interpolation Sea Surface Temperature (OISST.v2)
300 0.25° high resolution dataset from the National Oceanic and Atmospheric Administration
301 (Huang et al., 2021). Using this dataset compared to others has been proven to be the most
302 suitable for our region of interest (Yu et al., 2023).

303

304 We obtained monthly Photosynthetically Available Radiation (PAR) from the same Globcolour
305 project at the same spatial and temporal resolution (0.04° and 8 days) as chla.

306

307 We used monthly averaged ERA5 reanalysis of zonal (u) and meridional (v) surface wind speed
308 at 10 m above the surface (Hersbach et al., 2020).

309

310 We investigated monthly mean MLD from the Estimating the Circulation and Climate of the
311 Ocean (ECCO) ocean and sea-ice state estimate project (ECCO consortium et al., 2021). The
312 dataset is the version 4, release 4, at 0.5° spatial resolution.

313

314 Variability in the sea-ice landscape can be influenced by the Amundsen Sea Low (ASL) in West
315 Antarctica (Hosking et al., 2013; Turner et al., 2016). We therefore finally looked at the impact
316 of the ASL and its potential influence on sea-ice variability. Monthly ASL indices (latitude,
317 longitude, central and sector pressure) derived from ERA5 reanalysis data were obtained from
318 the ASL climate index page (Hosking et al., 2016).

319

320

Formatted: Font color: Text 1

Deleted: finally

Formatted: Font color: Text 1

Formatted: Font color: Text 1, Pattern: Clear (White)

Formatted: Left

322 2.6 Statistical analysis

323

324 Because some of our data were not normally distributed, we consistently applied nonparametric
325 tests throughout our statistical analysis. A Mann-Kendall test was performed to detect linear
326 trends in chla and NPP. A two-tailed non-parametric Spearman correlation metric (rho, p) was
327 calculated to investigate the relationship between chla, NPP, and environmental factors, as well
328 as between the phytoplankton bloom and sea-ice phenology metrics. A two-tailed Mann-Whitney
329 test was performed to detect any significant mean differences for chla, sea-ice phenology
330 metrics, MLD, PAR and dFe sources between the two polynyas. Monthly spatial correlations
331 were tested between SIC, winds, chla, NPP, SST, and PAR after removing the seasonality for
332 each parameter. As well, a yearly spatial correlation between chla, NPP and TVFall was
333 performed. The relationships between chla, NPP and environmental factors were explored using
334 a Principal Component Analysis (PCA). No pre-treatment (mean-centering or normalization)
335 was applied to the variables prior to PCA, as all variables are expressed in comparable units and
336 ranges, consistent with common practice in marine biogeochemistry studies (Marchese et al.,
337 2017; Liniger et al., 2020). The Spearman, Mann-Whitney and PCA analysis were conducted
338 using the mean TVFs, MLD, SST, and PAR calculated over the October-March period for each
339 year, with the associated bloom and sea-ice phenology metrics. Every statistical test was run with
340 a 95% (p-value < 0.05) confidence level. Our study spans 1998-2017. We are constrained by the
341 start of satellite ocean color data (1998) and the end of the ice shelf basal melt rate record (2017)
342 from Paolo et al (2023).

343

344 3. Results

345

346 3.1 Glacial meltwater, chla, and NPP variability

347

348 The annual climatology maps reveal substantially higher chla and NPP in the ASP compared to
349 the PIP (Fig. 2). Chla starts increasing in mid-November to reach its average peak earlier in the
350 PIP than the ASP. At its peak, chla in the ASP is 6.49 mg m^{-3} and 4.94 mg m^{-3} in the PIP (Fig.
351 3a). During the bloom period, chla is also higher in the ASP on average compared to the PIP
352 ($\text{ASP} = 5.21 \pm 1.29 \text{ mg m}^{-3}$; $\text{PIP} = 3.69 \pm 1.11 \text{ mg m}^{-3}$; p-value < 0.01; Fig. 3b; Supplementary

Deleted: glacial meltwater

Deleted: concentration

Formatted: Font color: Text 1

Deleted: chla

Deleted: concentration

Deleted: The chla concentration

Deleted: concentration

Deleted:

Deleted:,

361 Table T1). When looking at polynya area integrated values (concentration multiplied by area
 362 gives units of mg m^{-3}), chla is significantly higher in the ASP than in the PIP, and increases with
 363 the polynya area (Supplementary Figs. S1 and S2). NPP is also significantly higher in the ASP
 364 than in the PIP ($1.88 \pm 1.12 \text{ TgC y}^{-1}$ vs $0.85 \pm 0.86 \text{ TgC y}^{-1}$, p-value = 0.004; Supplementary
 365 Fig. S3). No significant interannual trends in mean chla and NPP during the bloom are observed
 366 for either polynya (p-value > 0.1; Fig. 3b; Supplementary Fig. S3). The climatological winter
 367 MLD in the ASP is deeper (MLD ASP = $45.8 \pm 8.0\text{m}$; MLD PIP = $36.4 \pm 7.3\text{m}$; p-value < 0.01;
 368 Fig. 1b), indicating that it may better entrain deeper sources of nutrients into the upper waters for
 369 the following phytoplankton growing season, resulting in higher productivity (Fig. 2).

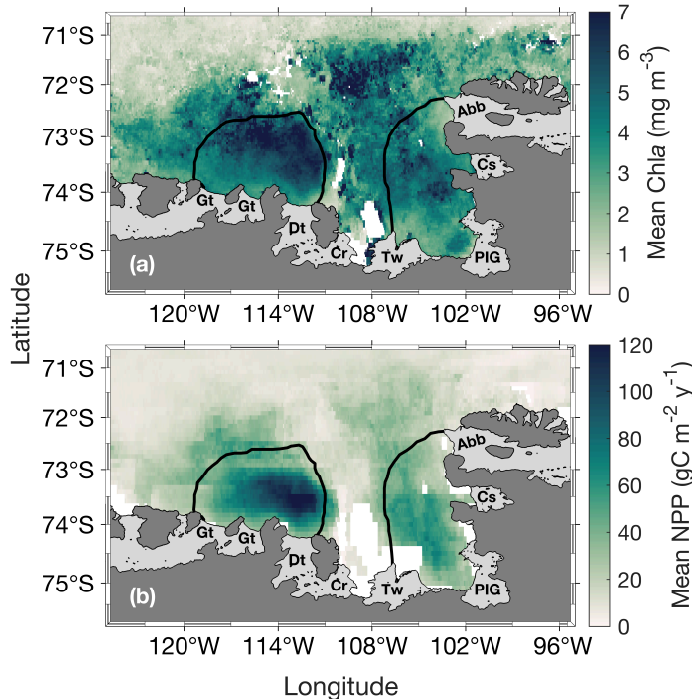
Deleted: : p-value < 0.01

Deleted: Fig. 3b; Supplementary Fig. S3; p-value > 0.1

Formatted: Font color: Text 1

Deleted: ¶

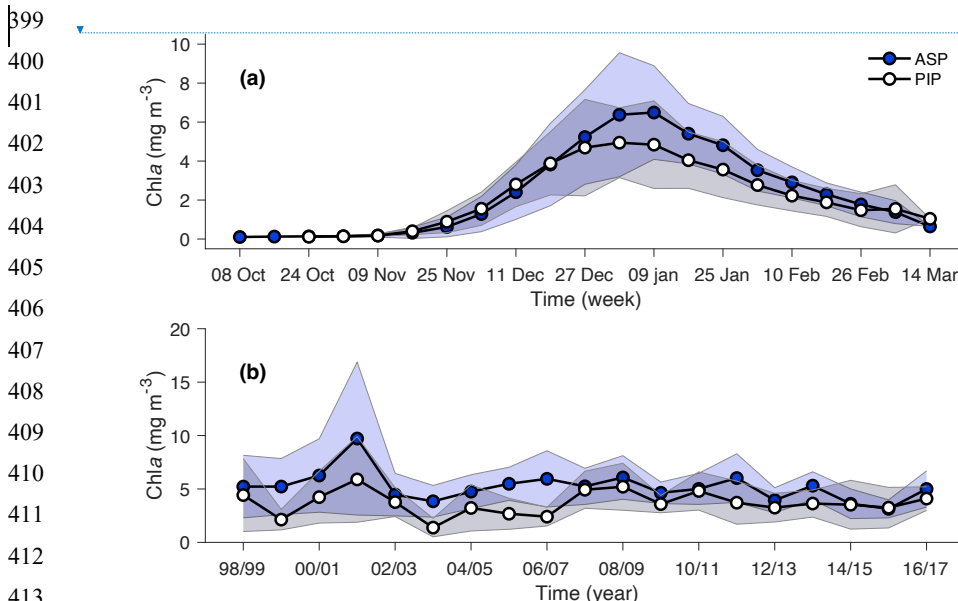
... [1]



389 **Fig. 2.** Spatial distribution of (a) mean surface chlorophyll-a (chl-a) concentration during the
 390 bloom and (b) net primary productivity (NPP) climatology (1998 – 2017) for the Amundsen

396 (ASP; [left](#)) and Pine Island (PIP; [right](#)) polynyas. The black lines represent the climatological
397 summer polynyas' boundaries.

398



Deleted: [2]

Formatted: Font: Bold

Formatted: Don't adjust right indent when grid is defined, Don't adjust space between Latin and Asian text, Don't adjust space between Asian text and numbers

Deleted: (

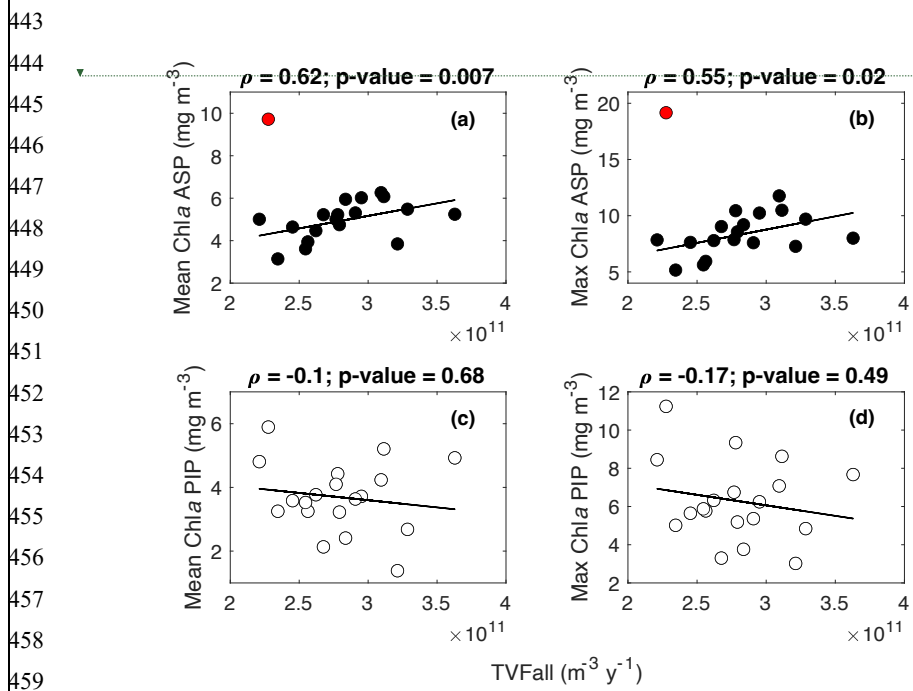
Deleted: (

Deleted:).

Deleted: concentration

Deleted: max

441 is delivered to the embayment. No strong relationships are observed in the PIP between TVFall,
 442 surface chla and NPP (Figs. 4c-d; Supplementary Figs. S4c-d).



Moved (insertion) [1]

461 [Fig. 4. Scatter plots of mean and maximum \(max\) surface chlorophyll-a \(chla\) concentrations](#)
 462 [with the total volume flux \(TVFall\) for \(a-b\) the Amundsen \(ASP\) and \(c-d\) the Pine Island](#)
 463 [\(PIP\) polynyas from 1998 to 2017 \(n=19\). The fitted lines and statistics exclude year 2001/02](#)
 464 [\(red outlier\) for the ASP regressions. If all data is considered, the relationships between mean](#)
 465 [chla, max chla and TVFall in the ASP are not significant. TVFall is an annual integral](#)
 466 [representing the sum of all ice shelves \(see methods section\) for the Amundsen Sea Embayment](#)
 467 [\(ASE\).](#)

Moved (insertion) [2]

468 When fluxes from individual glaciers are considered, PIP chla does not correlate with Abbot,
 469 Cosgrove, PIG, Thwaites or TVFpip fluxes (Table 1). On the other hand, ASP chla shows strong
 470 relationships with TVFasp, the Dotson and Crosson ice shelves (Table 1), and all ice shelves

472 become significantly correlated with mean and maximum chla when year 2001/02 is removed.
 473 There are no statistically significant relationships between individual ice shelves and NPP in
 474 either polynyas.
 475

Deleted: max

476 **Table 1.** Statistical summary (Spearman's rank correlation) of the relationships between ice
 477 shelves volume flux, mean and maximum (max) surface chlorophyll-a (chla) concentrations
 478 (n=19) in both polynyas. The * marks a significant (p-value < 0.05) relationship. All relationships
 479 between mean chla, maximum chla and ASP ice shelves become significant when year 2001/02 is
 480 removed.

Moved down [3]: chla are strongly correlated with TVFall in southern-eastern part of the ASP, in front of the Dotson ice shelf (Figs. 5a-b), where a positive relationship with NPP is also observed (Fig. 5c), although not significant.

Deleted: both polynyas. Spatially, the mean and max

481

	Amundsen Sea polynya (ASP)				Pine Island polynya (PIP)			
	Mean chla		Max chla		Mean chla		Max chla	
	rho	p-value	rho	p-value	rho	p-value	rho	p-value
Abbot	/	/	/	/	0.09	0.73	-0.04	0.88
Cosgrove	/	/	/	/	-0.32	0.18	-0.46	0.05
PIG	/	/	/	/	-0.04	0.88	-0.13	0.61
Thwaites	0.16	0.52	0.11	0.66	0.12	0.63	0.09	0.71
Crosson	0.43	0.07	0.50	0.03*	/	/	/	/
Dotson	0.48	0.04*	0.54	0.02*	/	/	/	/
Getz	0.37	0.12	0.43	0.07	/	/	/	/
TVFasp	0.42	0.07	0.46	0.05*	/	/	/	/
TVFpip	/	/	/	/	0.009	0.97	-0.1	0.68

Fig. 4. Scatter plots

Formatted: Normal (Web)

Deleted: with the total volume flux (TVFall) for (a-b) the ASP and (c-d) the PIP from 1998 to 2017

Moved up [2]: The fitted lines and statistics exclude year 2001/02 (red outlier) for the ASP regressions. If all data is considered, the relationships between mean chla, max chla and TVFall

Moved up [4]: Table 1.

Deleted:).

Deleted: the ASP are not significant. TVFall is an annual integral representing the sum of all ice shelves (see methods section) for the ASE.¶

¶

Deleted: Statistical summary of the relationships between ice shelves volume flux and¶ surface chlorophyll-a (chla).

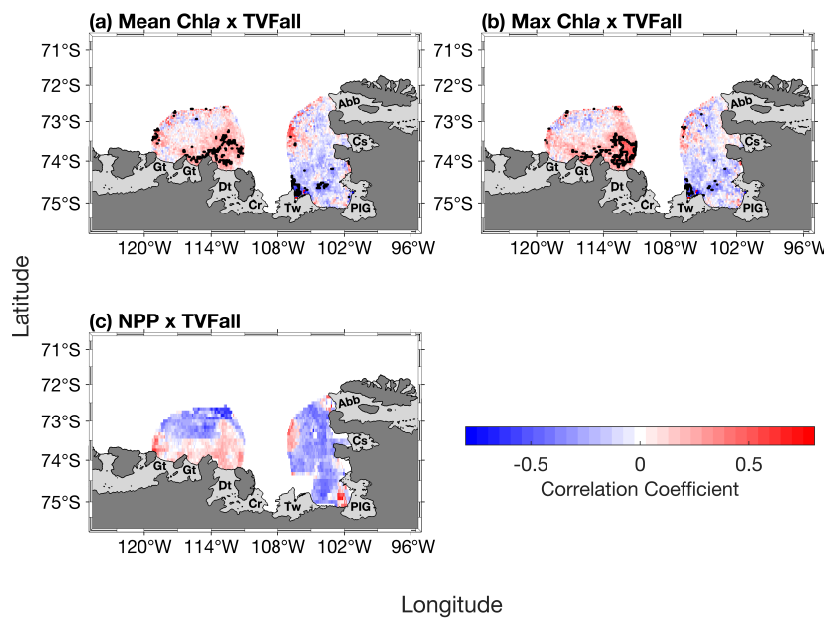
Deleted: Statistical results for the ASP include all years (n=19).

Deleted: max

Formatted Table

526 Spatially, the mean and maximum chla are strongly correlated with TVFall in southern-eastern
 527 part of the ASP, in front of the Dotson ice shelf (Figs. 5a-b), where a positive relationship with
 528 NPP is also observed (Fig. 5c), although not significant.

Moved (insertion) [3]



Deleted: ¶

<object>

547 **Fig. 5.** Spatial correlation maps between total volume flux (TVFall) and (a) surface mean
 548 chlorophyll-a (chla) concentration, (b) surface maximum (max) chla concentration and (c) net
 549 primary productivity (NPP) (n=19). The black contour represents significant correlations at 95%
 550 confidence level. Data outside of the summer climatological polynyas' boundaries were masked
 551 out.

Moved up [1]: ¶

552 3.2 Simulated dFe sources distribution

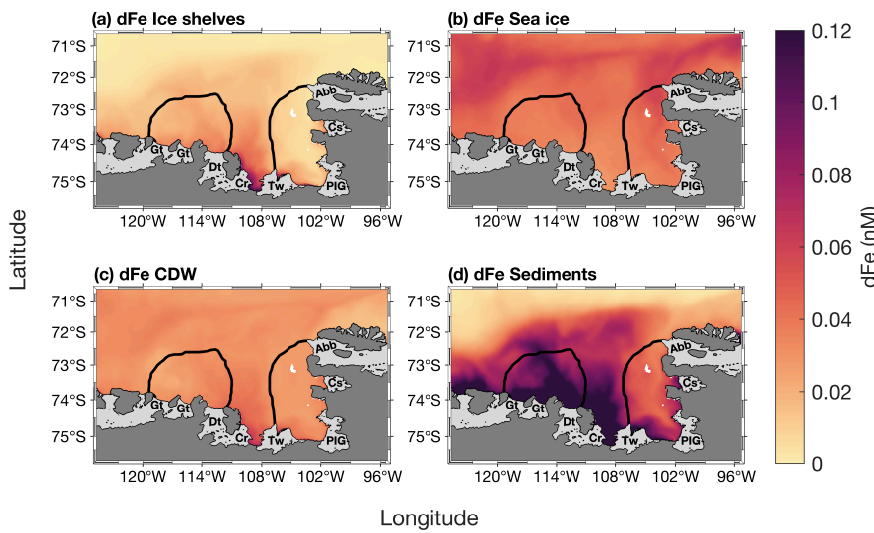
553 The modelled spatial distribution of surface dFe sources is presented in Fig. 6. On average, the
 554 smallest dFe source in the embayment is from the ice shelves, with a maximum concentration

Fig. 5

Deleted: 5.

Deleted:),

600 between the Thwaites and Dotson ice shelves. The dFe from sea ice is slightly higher than from
 601 ice shelves and similar over the two polynyas, and is higher near the sea-ice margin (Fig. 6b). The
 602 dFe from CDW is also higher between the Thwaites and Dotson (Fig. 6c). Sediment is the
 603 dominant dFe source (Fig. 6d). Its distribution spreads from 108°W to the western part of the Getz
 604 ice shelf. The highest sediment-sourced dFe concentration is found along the coast and inside the
 605 ASP. On polynya-wide average basis, the sediment reservoir contributes significantly more to total
 606 dFe in the ASP (58.3%, 0.13nM) compared to sea ice (16.5%, 0.04nM), CDW (13.5%, 0.03nM)
 607 and ice shelves (11.7%, 0.03nM). In the PIP, the contribution of sediments is still significantly
 608 higher (41.2%; 0.08nM) but lower than the ASP and the contribution gap with the other sources
 609 decreases. The CDW and sea ice contribute 22.5% (0.04nM) and 18.9% (0.035nM) to the dFe pool
 610 respectively, while ice shelves are still the smallest sources at 14.5% (0.03nM) in the PIP.



626 **Fig. 6.** Two-years top-100m averaged spatial distribution of surface dissolved iron (dFe)
 627 contribution from (a) ice shelves, (b) sea ice, (c) circumpolar deep water (CDW) and (d) sediments
 628 simulated by the model from Dinniman et al. (2020). The black lines represent the climatological
 629 summer polynyas' boundaries.

630

Deleted: <object>

Formatted: Font color: Text 1

Formatted: Font color: Text 1

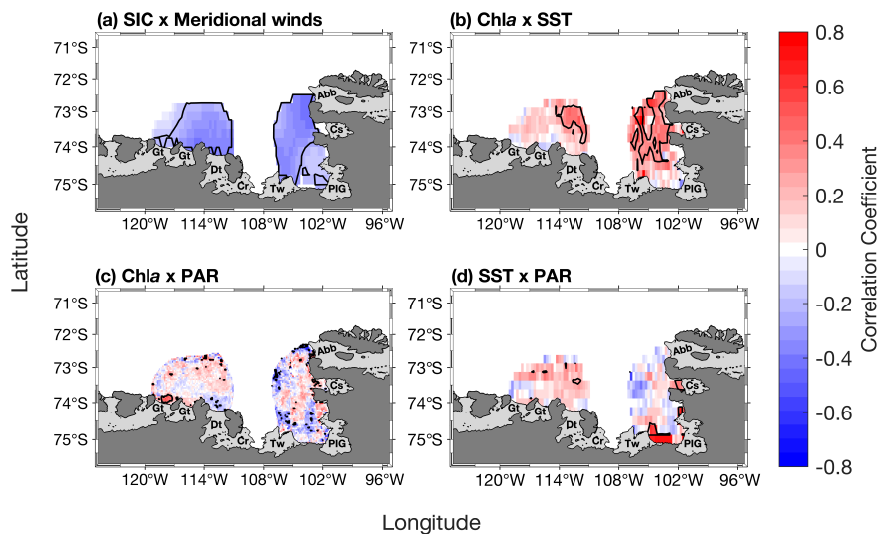
Formatted: Font color: Text 1

632 3.3 Environmental parameters, chla and NPP variability

633

634 During the phytoplankton growth season (October-March), SIC is spatially significantly
635 anticorrelated to the meridional winds speed in both polynyas (Fig. 7a). Chla is significantly
636 positively correlated with SST in the eastern ASP, and the whole PIP (Fig. 7b), but weakly with
637 PAR in both polynyas (Fig. 7c). Finally, PAR and SST are positively related in both central
638 polynyas, albeit not significantly (Fig. 7d). We note that similar spatial relationships are
639 observed when NPP is correlated with SST and PAR (Supplementary Fig. S5).

640



641

642 **Fig. 7.** Spatial correlation map between sea-ice concentration (SIC) and (a) meridional winds.
643 Spatial correlation maps between mean chlorophyll-*a* (chla) concentration and (b) sea surface
644 temperature (SST), (c) photosynthetically available radiation (PAR). (d) Spatial correlation map
645 between PAR and SST. Data span 1998 – 2017 from October to March (n=114). The black contour
646 represents significant correlations at 95% confidence level. Seasonality was removed before
647 performing the correlation. Data outside of the summer climatological polynyas' boundaries were
648 masked out.

649

Deleted: .

Deleted: <object>||

Formatted: Font: Bold

Formatted: Normal (Web), Justified

Deleted: from the data

Formatted: Normal (Web)

666 Regarding the phenology, the bloom start is positively correlated to IRT and negatively with
 667 OWP in the ASP, although not significantly with the OWP (Table 2). This means that the bloom
 668 starts earlier and later as IRT does, and that longer OWP and earlier bloom starts are correlated
 669 with earlier ice retreat. The bloom mean and bloom maximum (max) chla are not correlated with
 670 either IRT and OWP in the ASP. IRT and OWP are significantly related ($p = -0.93$; p-value <
 671 0.001). When year 2001/02 is removed, no significant changes in the relationships between all
 672 parameters are detected. In the PIP, all metrics are significantly related to each other, except for
 673 PAR and OWP (Table 2). That is, the bloom start is positively correlated with IRT and
 674 negatively with OWP, while the bloom duration, mean chla, max chla and NPP are negatively
 675 linked to the IRT and positively with OWP. SST and PAR are negatively correlated with IRT,
 676 and positively with SST. IRT and OWP are significantly related in the PIP ($p = -0.88$; p-value <
 677 0.001).

678

679 **Table 2.** Statistical summary ([Spearman's rank correlation](#)) of the relationships between the sea-
 680 ice phenology metrics and environmental parameters (n=19) in both polynyas. The * marks a
 681 significant (p-value < 0.05) relationship. IRT = ice retreat time, OWP = open water period, NPP =
 682 net primary productivity, SST = sea surface temperature, PAR = photosynthetically available
 683 radiation. Removing year 2001/02 for the ASP slightly changes the strength of the relationships
 684 between parameters (i.e., rho) but not the significance.

685

	Amundsen Sea polynya (ASP)				Pine Island polynya (PIP)			
	IRT		OWP		IRT		OWP	
	rho	p-value	rho	p-value	rho	p-value	rho	p-value
Bloom start	0.51	0.03*	-0.43	0.07	0.56	0.02*	-0.48	0.04*
Bloom duration	-0.12	0.63	0.09	0.71	-0.56	0.02*	0.59	0.01*
Bloom mean	0.19	0.44	-0.33	0.17	-0.67	0.003*	0.50	0.04*
Bloom max	0.24	0.32	-0.35	0.14	-0.65	0.005*	0.52	0.03*
NPP	-0.55	0.02*	0.45	0.05	-0.72	0.001*	0.54	0.02*

Deleted: concentrations

Deleted: phytoplankton bloom

Deleted:).

SST	-0.09	0.72	-0.01	0.96	-0.57	0.02*	0.52	0.03*
PAR	-0.09	0.72	0.05	0.84	-0.62	0.007*	0.38	0.12

692

693 We explore the relationships between phytoplankton bloom phenology metrics and their
 694 potential environmental drivers by conducting a multivariate PCA for both polynyas (Fig. 8).
 695 The PCA reduces our datasets (11 variables) and breaks them down into dimensions that capture
 696 most of the variability and relationships between all variables. Arrows indicate the contribution
 697 of each variable to the dimensions, with longer arrows representing stronger influence.
 698 Observations (in our case, years) positioned in the direction of an arrow are more influenced by
 699 that variable. In the ASP (Fig. 8a), the first two principal components explain 55.3% of the total
 700 variance (Dim1: 35%, Dim2: 20.3%). NPP in the ASP is closely associated with BD, indicating
 701 that the bloom duration is the primary driver of production. On the other hand, environmental
 702 vectors such as TVFall and TVFasp project more strongly onto Dim2 with the bloom mean chla,
 703 indicating that meltwater input may influence surface chla interannual variability, and is less
 704 directly tied to NPP. We note that when year 2001/02 is removed, the relationship between
 705 TVFasp and TVFall becomes much stronger with BM (Supplementary Fig. S6a) and is slightly
 706 anticorrelated to SST and MLD. In the PIP (Fig. 8b), the first two components account for 63.7%
 707 of the total variance (Dim1: 46.7%, Dim2: 17%). Compared to the ASP, both NPP and BM
 708 cluster strongly with BD and PAR on Dim1. Additionally, IRT, OWP and SST and MLD aligned
 709 along Dim1, which explains 46.7% of the total variance compared to 35% for the ASP,
 710 suggesting that physical conditions might play a stronger structuring role in PIP compared to the
 711 ASP. In contrast, TVFall and TVFpip stand alone and align more strongly with Dim2, suggesting
 712 a less dominant influence of meltwater on BM and NPP variability in the PIP. The summer
 713 polynya-averaged PAR and MLD are significantly stronger and deeper, respectively, in the ASP
 714 compared to the PIP during the bloom season (MLD ASP = 28.5 ± 5.7 m; MLD PIP = $24.9 \pm$
 715 3.7 m; p-value = 0.03 and PAR ASP = 31.5 ± 5.4 Einstein $m^{-2} d^{-1}$; PAR PIP = 26.5 ± 6.7 Einstein
 716 $m^{-2} d^{-1}$; p-value = 0.02).

Deleted: 

... [3]

782
783
784
785
786
787
788
789
790
791
792
793
794
795
796
797
798
799
800
801
802
803
804
805

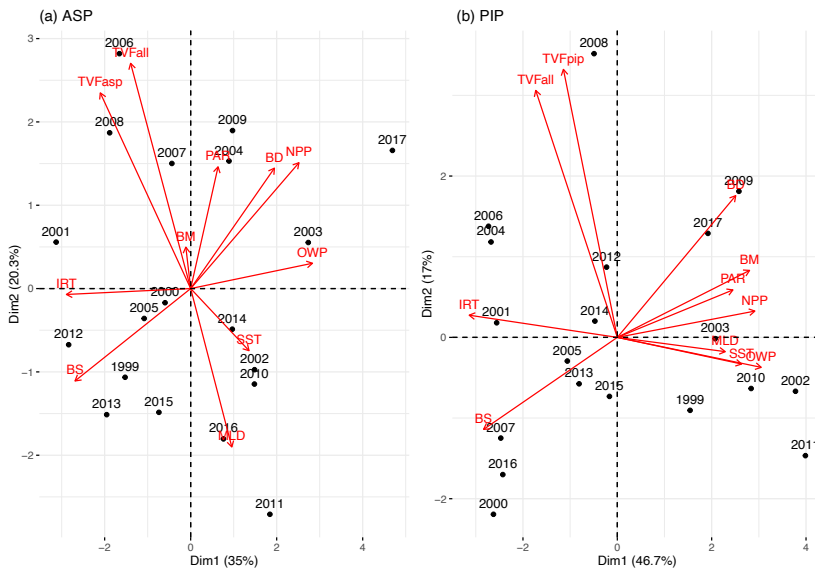


Fig. 8. Principal component analysis biplot of environmental parameters (red) and years (black) for (a) the [Amundsen \(ASP\)](#) and (b) the [Pine Island \(PIP\) polynyas](#). TVFasp = total volume flux for ASP; TVFpip = total volume flux for PIP; TVFall = total volume flux for all ice shelves; BM = bloom mean; PAR = photosynthetically available radiation; BD = bloom duration; NPP = net primary productivity; OWP = open water period; SST = sea surface temperature; MLD = mixed-layer depth; BS = bloom start; IRT = ice retreat time. The same plot is presented in supplementary Fig. S6, but removing year 2001/02 for the ASP, emphasizing the relationship between total volume flux (TVFall, TVFasp) and BM in the ASP.

Finally, we find on average weak spatial negative relationships between SIC and ASL latitude, longitude, mean sector and actual central pressure in both polynyas during the growing season (Supplementary Fig. S7), and only slightly significant in the eastern PIP.

Formatted: Font color: Black

Formatted: Normal (Web), Justified, Automatically adjust right indent when grid is defined, Adjust space between Latin and Asian text, Adjust space between Asian text and numbers

813 **4. Discussion**

814

815 4.1 Effect of glacial meltwater on phytoplankton chla and NPP

816

817 The relationship between glacial meltwater, surface chla and NPP observed over the last two
818 decades was distinctly different between the two polynyas. In the ASP, we found that enhanced
819 glacial meltwater translates into higher surface chla, but not with NPP (when removing year
820 2001/02; Figs. 4a-b; Supplementary Fig. S6a). Modelling results (Fig. 6) suggest that sediment
821 from the seafloor is the main source of dFe in the ASP, but this source is also linked to glacial
822 melt. Ice shelf glacial meltwater drives the meltwater pump, which brings up mCDW and fine-
823 grained subglacial sediments to the surface. This result is in agreement with previous research:
824 Melt-laden modified CDW flowing offshore from the Dotson ice shelf to the central ASP
825 (Sherrell et al., 2015), and resuspended sediments (Dinniman et al., 2020; St-Laurent et al., 2017;
826 2019) have been identified as significant sources of dFe to be used by phytoplankton.
827 Interestingly, both dFe supplied from ice shelves and CDW are most important in front of the
828 Thwaites and Crosson ice shelves, where the area averaged basal melt rate, and thus likely the
829 area averaged meltwater pumping (Jourdain et al., 2017), are typically strongest in observations
830 (Adusumilli et al., 2020; Rignot et al., 2013) and modelling (Fig. 6). The year 2001/02 does not
831 stand out as being influenced by any specific parameter in the ASP compared to other years (Fig.
832 8a, Supplementary Fig. S6a). The anomalously high surface chla observed during this year, as
833 also reported by Arrigo et al. (2012), may result from exceptional conditions that were not
834 captured by the parameters analysed in our study, for instance, an imbalance in the grazing
835 pressure. Interestingly, surface chla and NPP exhibit contrasting trends when averaged across the
836 polynya. While TVFall may explain some of the variance in surface chla, it does not account for
837 the variance in NPP, whether assessed through direct or multivariate relationships. This
838 decoupling between chla and NPP in the ASP suggests that glacial meltwater, while enhancing
839 surface phytoplankton biomass through nutrient delivery, may also promote vertical mixing. This
840 mixing deepens the mixed layer, reducing light availability and constraining photosynthetic
841 rates. These rates are influenced by fluctuations in the MLD, even in the presence of high
842 biomass and sufficient macronutrients. The summer MLD is deeper in the ASP, which would
843 decrease light availability, despite higher PAR compared to the PIP. Previous studies report that

Deleted: melt

Formatted: Font color: Text 1

Deleted: the

Formatted: Font color: Text 1

Deleted: (Fig. 1b),

Formatted: Font color: Text 1

847 the small prymnesiophyte *P. antarctica*, a low-efficiency primary producer (Lee et al., 2017), is
848 better adapted to deeper mixed layers and therefore lower light conditions (Alderkamp et al.,
849 2012; Mills et al., 2010) and could contribute to high surface chla decoupled from NPP, as
850 observed in the ASP. This is consistent with past *in situ* studies showing systematic differences
851 in mixed-layer structure between the two polynyas. The PIP commonly exhibits a shallow,
852 strongly stratified surface mixed layer while the ASP is more variable and has been observed to
853 host deeper MLD (Alderkamp et al., 2012; Park et al., 2017; Yager et al., 2016; Mills et al.,
854 2012). [Near glacier and ice-shelf fronts, entrainment of iron-rich deep waters rising to the surface](#)
855 [through the meltwater pump can also produce surface chla maxima \(high biomass from. *P.*](#)
856 [antarctica\) without proportional increases in depth-integrated productivity due to self-shading](#)
857 [\(Twelves et al., 2021\)](#). Further from the coast, meltwater spreading at neutral buoyancy
858 strengthens stratification, limiting vertical nutrient fluxes and thereby suppressing NPP despite
859 elevated chla. These dual mechanisms are consistent with observational and modelling studies of
860 meltwater entrainment and dispersal (Randall-Goodwin et al., 2015; St-Laurent et al., 2017;
861 Dinniman et al., 2020; Forsch et al. 2021), and suggest that spatial heterogeneity in plume
862 dynamics could explain the observed chla and NPP mismatch.

863
864 In the PIP, we did not find any long-term relationships between the phytoplankton bloom, NPP
865 and glacial meltwater. Variability in ice shelf glacial meltwater may not have the same effect on
866 the surface chla and NPP in the PIP compared to the ASP. Iron delivered from glacial melt
867 process related in the PIP and west of it could accumulate and follow the westward coastal
868 current, towards the ASP (St-Laurent et al., 2017). These sources would include dFe from
869 meltwater pumped CDW, sediments and ice shelves, all of which are higher in front of the
870 Crosson ice shelf, west of the PIP (Fig. 6). With the coastal circulation, this would make dFe
871 supplied by glacial meltwater greater in the ASP, thereby contributing to the higher productivity
872 in the ASP. [Recently, subglacial discharge \(SGD\) was shown to have a different impact on basal](#)
873 [melt rate in the ASE polynyas \(Goldberg et al., 2023\)](#), where PIG had a lot less relative increase
874 in melt with SGD input than Thwaites or Dotson/Crosson. Thus, assuming a direct relationship
875 between meltrate, SGD and dFe sources, the signal in the PIP (fed by PIG melt) will be much
876 weaker than in the ASP (fed by upstream Thwaites, Crosson and local Dotson due to the
877 circulation), which might also explain the discrepancies between the PIP and ASP. A stronger

Moved (insertion) [5]

Formatted: Font color: Text 1

878 meltwater-driven stratification may also dominate in the PIP, reducing vertical nutrient
879 replenishment and thereby limiting biomass growth (Oh et al., 2022), even where TVFall is high,
880 hence leading to a direct negative relationship observed compared to the ASP (Fig. 4;
881 Supplementary Fig. S4). The model outputs used here are critical to understand the spatial
882 distribution of dFe in the embayment. They strongly suggest, but do not definitively demonstrate,
883 the role of dFe in influencing the phytoplankton bloom interannual variability.
884

885 Satellite algorithms commonly estimate NPP from surface chla, but the approach and
886 assumptions vary across models. The VGPM relates chla to depth-integrated photosynthesis
887 through empirical relationships with light and temperature (Behrenfeld & Falkowski, 1997). In
888 contrast, the Carbon-based Productivity Model (CbPM) emphasizes phytoplankton carbon
889 biomass and growth rates derived from satellite optical properties, decoupling productivity
890 estimates from chla alone (Westberry et al., 2008). The CAFE model (Carbon, Absorption, and
891 Fluorescence Euphotic-resolving model) integrates additional physiological parameters such as
892 chla fluorescence and absorption to better constrain phytoplankton carbon fixation (Silsbe et al.,
893 2016). In the Southern Ocean, where light limitation, iron supply, and community composition
894 strongly influence the relationship between chla and productivity, these algorithmic differences
895 can yield substantial variability in NPP estimates (Ryan-Keogh et al., 2023), with studies
896 showing that VGPM-type models often outperform CbPM in coastal Southern Ocean regions
897 (Jena et al., 2020). Because the VGPM algorithm does not explicitly incorporate the MLD, but
898 instead estimates primary production integrated over the euphotic zone based on surface chla,
899 PAR, and temperature, it may not fully capture the influence of variable MLD or subsurface
900 processes related to glacial melt, which could contribute to the observed decoupling between
901 chla and NPP. Therefore, while the observed decoupling between chla and NPP in the ASP
902 might also come from our choice of dataset, the VGPM model may be more appropriate for
903 coastal polynya environments, such as those in the Amundsen Sea. We finally note as a
904 limitation that satellite-derived chla and VGPM NPP estimates lack the vertical resolution
905 needed to resolve sub-plume stratification and mixing processes (e.g., fine-scale vertical
906 gradients in iron or nutrient fluxes), so our mechanistic interpretations of surface chla vs. depth-
907 integrated productivity decoupling must be taken with caution.
908 ▲

Formatted: Font color: Text 1

Formatted: Font color: Text 1

Moved up [5]: Further from the coast, meltwater spreading at neutral buoyancy strengthens stratification, limiting vertical nutrient fluxes and thereby suppressing NPP despite elevated chla. These dual mechanisms are consistent with observational and modelling studies of meltwater entrainment and dispersal (Randall-Goodwin et al., 2015; St-Laurent et al., 2017; Dinniman et al., 2020; Forsch et al. 2021), and suggest that spatial heterogeneity in plume dynamics could explain the observed chla and NPP mismatch.

Moved down [6]: note as a limitation that satellite-derived chla and VGPM NPP estimates lack the vertical resolution needed to resolve sub-plume stratification and mixing processes (e.g., fine-scale vertical gradients in iron or nutrient fluxes), so our mechanistic interpretations of surface chla vs. depth-integrated productivity decoupling must be taken with caution.

Deleted: The decoupling between surface chla and NPP could reflect two contrasting meltwater effects. Near glacier and ice-shelf fronts, entrainment of iron-rich deep waters rising to the surface through the meltwater pump can produce surface chla maxima (high biomass) without proportional increases in depth-integrated productivity.

Deleted: We also

Deleted: ▲

Formatted: Font color: Text 1

Moved (insertion) [6]

Formatted: Font color: Text 1

934 Direct observations from Sherrell et al. (2015) showed higher chla in the central ASP while
935 surface dFe was low weeks before the bloom peak. This suggests a continuous supply and
936 consumption of dFe in the area, most likely from the circulation, as mentioned earlier.
937 Considering the long residence time of water masses in both polynyas (about 2 years (Tamsitt et
938 al., 2021)), and the daily dFe uptake by phytoplankton (3-196 pmol l⁻¹ d⁻¹ (Lannuzel et al.,
939 2023)), we also hypothesise that any dFe reaching the upper ocean from external sources is
940 quickly used and unlikely to remain readily available for phytoplankton in the following spring
941 season.

942
943 In recent model simulations with the meltwater pump turned off, Fe becomes the principal factor
944 limiting phytoplankton growth in the ASP (Oliver et al., 2019). However, the transport of Fe-rich
945 glacial meltwater outside the ice shelf cavities and to the ocean surface depends strongly on the
946 local hydrography. While Naveira Garabato et al. (2017) suggested that the glacial meltwater
947 concentration and settling depth (neutral buoyancy) outside the ice shelf cavities is controlled by
948 an overturning circulation driven by instability, others suggest that the strong stratification plays
949 an important role in how close to the surface the buoyant plume of said meltwater can rise
950 (Arnscheidt et al., 2021; Zheng et al., 2021). Therefore, high melting years and greater TVFall
951 might not necessarily translate into a more iron-enriched meltwater delivered to the surface
952 outside the ice shelf cavities, close to the ice shelf edge, as rising water masses may be either
953 prevented from doing so, or be transported further offshore in the polynyas where the
954 phytoplankton bloom occurs, before they can resurface (Herraiz-Borreguero et al., 2016).

955
956 Although several Fe sources can fuel polynya blooms, and they depend on processes mentioned
957 above, Fe-binding ligands may ultimately set the limit on how much of this dFe stays dissolved
958 in the surface waters (Gledhill and Buck, 2012; Hassler et al., 2019; Tagliabue et al., 2019).
959 Models of the Amundsen Sea (Dinniman et al., 2020, 2023; St-Laurent et al., 2017, 2019) did not
960 include Fe complexation with ligands and assumed a continuous supply of available dFe for
961 phytoplankton. Spatial and seasonal data on Fe-binding ligands along the Antarctic coast remain
962 extremely scarce and their dynamics are poorly understood (see Smith et al. (2022) for a
963 database of publicly available Fe-binding ligand surveys performed south of 50°S). Field
964 observations in the ASP and PIP suggest that the ligands measured in the upwelling region in

Formatted: Font color: Text 1

Deleted: circulation

Deleted: above

Formatted: Font color: Text 1

967 front of the ice shelves had little capacity to complex any additional Fe supplied from glacial
968 melt. As a consequence, much of the glacial and sedimentary Fe supply in front of the ice
969 shelves could be lost via particle scavenging and precipitation (Thuróczy et al., 2012). This was
970 also observed by van Manen et al. (2022) in the ASP. However, within the polynya blooms,
971 Thuróczy et al. (2012) found that the ligands produced by biological activity were capable of
972 stabilising additional Fe supplied from glacial melt, where we observed the highest productivity.
973 The production of ligands by phytoplankton would increase the stock of bioavailable dFe and
974 further fuel the phytoplankton bloom in the polynyas, potentially highlighting the dominance
975 of *P. antarctica*, which uses iron-binding ligands more efficiently than diatoms (Thuróczy et al.,
976 2012), even under low light conditions. Model development and sustained field observations on
977 dFe availability, including ligands, are needed to adequately predict how these may impact
978 biological productivity under changing glacial and oceanic conditions, now and in the future.
979

980 Overall, the discrepancies observed between the ASP and PIP point to a complex set of ice-
981 ocean-sediment interactions, where several co-occurring processes and differences in
982 hydrographic properties of the water column influence dFe supply and consequent primary
983 productivity.

984
985 4.2 Possible drivers of the difference in phytoplankton surface chla and NPP between the
986 two polynyas

987 The biological productivity is higher in the ASP than the PIP, consistent with previous studies
988 (Arrigo et al., 2012; Park et al., 2017). In section 4.1, we mentioned the suspected underlying
989 hydrographic drivers of these differences. We related the higher biological productivity in the
990 ASP to a potentially greater supply of iron from melt-laden dFe-enriched mCDW and sediment
991 sources, but this difference in productivity could also be attributed to other local features. The
992 Bear Ridge grounded icebergs on the ASP's eastern side (Bett et al., 2020) could add to the
993 overall meltwater pump strength. They can enhance warm CDW intrusions to the ice shelf cavity
994 (Bett et al., 2020), increasing ice shelf melting and subsequent stronger phytoplankton bloom
995 from the meltwater pump activity. These processes are weaker or absent in the PIP. Few sources
996 other than glacial meltwater may influence the bloom in the PIP. For instance, dFe in the

Formatted: Font color: Text 1
Formatted: Font color: Text 1
Deleted: recently
Formatted: Font color: Text 1
Deleted:
Formatted: Font color: Text 1

Formatted: Font color: Text 1
Formatted: Font color: Text 1
Formatted: Font color: Text 1
Deleted: Fe
Formatted: Font color: Text 1
Formatted: Font color: Text 1

1001 euphotic zone can also be sustained by the biological recycling, as shown in the PIP by Gerringa
1002 et al. (2020).

Formatted: Font color: Text 1

Formatted: Font color: Text 1

1003
1004 Sea ice could also partly explain the difference in chla magnitudes, NPP, and variability between
1005 the ASP and PIP. The strong spatial correlation between SIC and meridional winds (Fig. 7a)
1006 indicates that southerly winds can export the coastal sea ice offshore and play a significant role
1007 in opening the polynyas. In the ASP compared to the PIP, sea ice retreats earlier (IRT = Jan 1st ±
1008 14d vs Jan 18th ± 17d, p-value = 0.003), the open water period is longer (OWP = 61 ± 16d vs 44
1009 ± 22d, p-value < 0.001), and the SIC is lower (Supplementary Fig. S8). In the ASP, an early sea-
1010 ice retreat leads to an earlier bloom start, but the longer open water period is not significantly
1011 associated with greater bloom mean or maximum chla (Table 2). On the other hand in the PIP,
1012 an early sea-ice retreat also triggers an early bloom start, but the longer open duration is
1013 associated with warmer water, higher bloom mean chla, maximum chla, and NPP. These results
1014 suggest that different processes might drive phytoplankton growth variability in the two
1015 polynyas. In the ASP, it is likely the replenishment of dFe mentioned above that mostly
1016 influences the bloom. In the PIP, higher SIC can delay the retreat time and shorten the open
1017 water season (Table 2, Supplementary Fig. S8), leading to lower chla and NPP compared to the
1018 ASP. The significant negative relationships between IRT, PAR, chla and NPP in the PIP (Table
1019 2, Supplementary Fig. S6) suggests a strong light limitation relief in the polynya. This light
1020 limitation hypothesis is further supported by the high correlation between polynya-averaged chla
1021 mean with PAR and SST in the PIP across the 19 years of study, compared to the lack of
1022 correlation in the ASP (Supplementary Table T2; p-value < 0.01 for all relationships in the PIP).

Deleted: S7

Deleted: and max

Deleted: max

Deleted: S7

1023 While *P. antarctica* is usually the main phytoplankton species dominating in both polynyas, the
1024 combination of light-limitation relief and higher SST may create better conditions for a stratified
1025 and warmer environment that would favor diatom (Arrigo et al., 1999; van Leeuwe et al., 2020),
1026 as recently observed in the ASP (Lee et al., 2022). The positive association of PAR, SST and
1027 chla with MLD likely reflects conditions around sea-ice retreat (all negatively associated with
1028 IRT), when enhanced wind mixing deepens the mixed layer and replenishes surface nutrients
1029 while light availability and SST increases. This nutrient-light co-limitation phase supports high
1030 biomass accumulation, likely from diatoms. Similar results have been reported by Park et al.
1031 (2017). They found that the PIP was dFe was not limited by dFe, potentially from biological

Formatted: Font color: Text 1

Deleted: replete

Formatted: Font color: Text 1

1037 recycling (Gerringa et al., 2020), compared to an iron-limited ASP. We hypothesise that the
1038 connection between glacial meltwater and chla that we found in the ASP is a response to iron
1039 input (also observed by Park et al. (2017) during incubation experiments) compared to the PIP,
1040 where light and temperature seem to play a more significant role in driving the phytoplankton
1041 bloom variability. Hayward et al. (2025) showed a decline in diatoms from 1997 to 2017 in the
1042 PIP. However, they observed an increase in diatoms after 2017, linked to regime shift in sea ice.
1043 Their study also indicates that diatoms are competitively disadvantaged under iron-depleted
1044 conditions. *P. antarctica*, which relies on dFe supplied by ocean circulation, would then tend to
1045 dominate in the ASP. Such shifts in phytoplankton composition are likely to affect carbon
1046 export, grazing, and higher trophic levels. Additional long-term data on inter-annual variability
1047 in phytoplankton composition and physiology will be essential to fully understand these
1048 relationships.

1049

1050 Finally, the weak relationships between the ASL indices and SIC might be owing to the seasonal
1051 variation of the ASL, where its position largely varies during summer, and its impact in shaping
1052 coastal sea ice is also greater during winter and autumn in the Amundsen-Bellingshausen region
1053 (Hosking et al., 2013). The lack of strong significant relationships overall does not allow us to
1054 conclude that the ASL plays an important role in shaping the coastal polynyas landscape and
1055 influencing chla variability.

1056

1057 4.3 Limitations and future directions

1058

1059 We acknowledge that elevated concentrations of suspended sediments (and non-
1060 photosynthetically active particles in general) near the ocean surface can impart optical
1061 signatures that bias satellite-derived chla high in coastal waters. Consequently, the higher chla
1062 observed in the ASP relative to the PIP, as well as the weak correspondence between chla and
1063 NPP in ASP, may reflect some sediment-driven optical effects rather than enhanced
1064 phytoplankton biomass or productivity alone. While our results are consistent with known
1065 differences in iron supply and mixed-layer dynamics between the two polynyas, the potential
1066 contribution of sediment-related bias cannot be ruled out and should be acknowledged when
1067 interpreting spatial contrasts in satellite chla on the Antarctic shelf.

Deleted: (

Formatted: Font color: Text 1

Formatted: Font color: Text 1

Deleted: Our results suggest potential long-term changes in the phytoplankton community, specifically a shift towards diatoms in the ASE coastal regions during phytoplankton bloom. Hayward et al. (2025) reported

Formatted: Font color: Text 1

Deleted: tends

Formatted: Font color: Text 1

Formatted: Font color: Text 1

Deleted: Variability in SIC and sea-ice retreat can be influenced by the Amundsen Sea Low (ASL). We therefore also investigated its potential role on sea-ice variability. We found on average weak spatial negative relationships between SIC and ASL latitude, longitude, mean sector and actual central pressure in both polynyas during the growing seasons (Supplementary Fig. S8), and only slightly significant in the eastern PIP. The weak relationships

Formatted: Font color: Text 1

Formatted: Font color: Text 1

1082

1083 While it seems reasonable that the higher ASP productivity could be driven by more iron
1084 delivered through a stronger meltwater pump downstream of the PIP, our data cannot confirm
1085 this hypothesis. To accurately understand the role of iron through the meltwater pump process,
1086 we would need to quantify the fraction of meltwater and glacial modified water (mix of CDW
1087 and ice shelf meltwater) reaching the ocean surface, together with the iron content. Obtaining
1088 this information is challenging over the decadal time scales considered and the method used in
1089 our study. Here, our intention was to provide valuable insights into the potential drivers of our
1090 results, and highlight the benefit of remote sensing, in this poorly observed environment. Our
1091 work directly aligns with Pan et al. (2025), who investigated the long-term relationship between
1092 sea surface glacial meltwater and satellite surface chla in the Western Antarctic Peninsula, and
1093 found a strong relationship between the two parameters, highlighting the importance of glacial
1094 meltwater discharge in regions prone to extreme and rapid climate changes.

1095

1096 In multimodel climate change simulations, Naughten et al (2018) showed an increase of ice
1097 shelves melting up to 90% on average, attributed to more warm CDW on the shelf, due to
1098 atmospherically driven changes in local sea-ice formation. More recently, Dinniman et al. (2023)
1099 also highlighted the impact of projected atmospheric changes on Antarctic ice sheet melt. They
1100 showed that strengthening winds, increasing precipitation and warmer atmospheric temperatures
1101 will increase heat advection onto the continental shelf, ultimately increasing basal melt rate by
1102 83% by 2100. Compared to present climate simulations, their simulation showed a 62% increase
1103 in total dFe supply to shelf surface waters, while basal melt driven overturning Fe supply
1104 increased by 48%. The ice shelf melt and overturning contributions varied spatially, increasing in
1105 the Amundsen-Bellingshausen area and decreasing in East Antarctica. This implies that, under
1106 future climate change, phytoplankton productivity could show stronger spatial asymmetry
1107 around Antarctica. The increasing melting and thinning of ice shelves will eventually result in
1108 more numerous calving events and drifting icebergs (Liu et al., 2015). Model simulations
1109 stressed the importance of ice shelves and icebergs in delivering dFe to the SO (Death et al.,
1110 2014; Person et al., 2019), increasing offshore productivity. As Fe will likely be replenished and
1111 sufficient from increasing melting in coastal areas, it is possible that the system will shift from

Formatted: Font color: Text 1

1112 Fe-limited to being limited by nitrate, silicate, or even manganese (Anugerahananti and Tagliabue,
1113 2024), while offshore SO productivity will likely remain Fe-dependent (Oh et al., 2022).

Formatted: Font color: Text 1

1115 5. Conclusions

1116

1117 Using spatial and multivariate approaches, our study explored the variability of surface chla and
1118 NPP in the Amundsen Sea polynyas over the last two decades, with a focus on the main
1119 environmental characteristics of the ASE. We found a strong relationship between ice shelf
1120 melting and surface chla in the ASP when year 2001/02 was removed, a result in agreement with
1121 the ASPIRE field studies and previous satellite analyses. On the other hand, we did not find clear
1122 evidence of such a relationship in the PIP, where light, sea surface temperature and open water
1123 availability seem more important. The differences between the polynyas may lie in hydrographic
1124 properties, or the use of satellite remote sensing itself, which cannot tell us about processes such
1125 as Fe supply, bioavailability and phytoplankton demand. To gain greater insight, we referred to
1126 model simulations that showed the spatial variability in the magnitude of iron sources. Our
1127 results call for sustained *in situ* observations (e.g., moorings equipped with trace-metal clean
1128 samplers, and physical sensors to better understand year-to-year water mass meltwater fraction
1129 and properties) to elucidate these long-term relationships. Satellite observations are a powerful
1130 tool to investigate the relationship between glacial meltwater and biological productivity on such
1131 time scales, which has until now relied almost exclusively on field observations and modelling.
1132 Using such tools, we showed how the relationship between phytoplankton and the environment
1133 varies spatially and temporally across 19 years.

Deleted: potential

Deleted: , which becomes stronger

1134

1135 Appendices

1136 No appendices are related to the manuscript.

1137

1138 Data availability

1139 Bathymetry data (Amante & Eakins, 2009) was taken from the NOAA website
1140 (<http://www.ngdc.noaa.gov/mgg/global/global.html>). Mixed-layer depth (ECCO Consortium et
1141 al., 2021) can be accessed here:
1142 https://podaac.jpl.nasa.gov/dataset/ECCO_L4_MIXED_LAYER_DEPTH_05DEG_MONTHLY

Formatted: Font color: Text 1

1145 V4R4. Satellite surface chlorophyll-*a* and photosynthetically available radiation were
1146 downloaded from <https://www.globcolour.info/>. Sea surface temperature (Huang et al., 2021)
1147 can be found here <https://psl.noaa.gov/data/gridded/data.noaa.oisst.v2.highres.html>. Wind re-
1148 analysis data (Hersbach et al., 2020) are available at
1149 [https://cds.climate.copernicus.eu/datasets/reanalysis-era5-single-levels-monthly-
1150 means?tab=download](https://cds.climate.copernicus.eu/datasets/reanalysis-era5-single-levels-monthly-means?tab=download). Sea-ice concentration (Cavalieri et al., 1996) was obtained from
1151 <https://nsidc.org/data> and Net Primary productivity (Behrenfeld and Falkowski, 1997) was
1152 downloaded from http://sites.science.oregonstate.edu/ocean_productivity/index.php. Circumpolar
1153 surface model output from Dinniman et al (2020) can be found at [https://www.bco-
1154 dmo.org/dataset/782848](https://www.bco-dmo.org/dataset/782848). The Amundsen Sea Low index (Hosking et al., 2016) data are available
1155 at http://scotthosking.com/asl_index.

1156
1157 **Author contributions**
1158 GL conceptualised and led the study; MSD provided the dissolved iron model output. All authors
1159 were involved in the interpretation of the results, the revision, and the writing of the final version
1160 of the paper.

1161
1162 **Competing interest**
1163 We declare having no competing interests.

1164
1165 **Acknowledgments**
1166 We would like to thank the University of Tasmania, the Australian Research Council (ARC)
1167 Centre of Excellence for Climate Extremes (CE170100023), and the Australian Centre for
1168 Excellence in Antarctic Science (ACEAS; SR200100008) for financial support. Delphine
1169 Lannuzel is funded by the ARC through a Future Fellowship (L0026677). Sebastien Moreau
1170 received funding from the Research Council of Norway (RCN) for the project “I-CRYME:
1171 Impact of CRYosphere Melting on Southern Ocean Ecosystems and biogeochemical cycles”
1172 (grant number 335512) and for the Norwegian Centre of Excellence “iC3: Center for ice,
1173 Cryosphere, Carbon and Climate” (grant number 332635). Michael Dinniman was supported by
1174 the U.S National Science Foundation grant OPP-1643652. We are also grateful to Will Hobbs,
1175 Rob Massom and Patricia Yager for their knowledgeable input. We thank Vincent Georges for

Formatted: Font color: Text 1

1176 some preliminary work as part of his masters' internship. We are very grateful to Fernando S.
1177 Paolo for his early input and help with the glacial meltwater dataset. We thank the data providers
1178 mentioned in the methods section for making their data available and free of charge.

1179

1180 **Financial support**

1181 All financial support were mentioned in the Acknowledgment section.

1182

1183 **References**

1184 Adusumilli, S., Fricker, H. A., Medley, B., Padman, L., and Siegfried, M. R.: Interannual
1185 variations in meltwater input to the Southern Ocean from Antarctic ice shelves, *Nat. Geosci.*, 13,
1186 616–620, <https://doi.org/10.1038/s41561-020-0616-z>, 2020.

1187 Alderkamp, A-C., Mills, M. M., van Dijken, G. L., Lann, P., Thuróczy, C-E., Gerringa, L. J.A.,
1188 de Barr, H. J. W., Payne, C. D., Visser, R. J. W., Buma A. G. J., and Arrigo, K. R.: Iron from
1189 glaciers fuels phytoplankton blooms in the Amundsen Sea (Southern Ocean): Phytoplankton
1190 characteristics and productivity, *Deep-Sea Res. II.*, 71–76, 32–48,
1191 <https://doi.org/10.1016/j.dsr2.2012.03.005>, 2012.

1192

1193 Amante, C., and Eakins, B.W.: ETOPO1 1 Arc-Minute Global Relief Model: Procedures, Data
1194 Sources and Analysis, NOAA Technical Memorandum NESDIS NGDC-24. National
1195 Geophysical Data Center [data set], NOAA, doi:10.7289/V5C8276M, 2009.

1196

1197 Anugerahanti, P. and Tagliabue, A.: Response of Southern Ocean Resource Stress in a Changing
1198 Climate, *Geophys. Res. Lett.*, 51, e2023GL107870, <https://doi.org/10.1029/2023GL107870>,
1199 2024.

1200 Ardyna, M., Claustre, H., Sallée, J-B., D'Ovidio, F., Gentili, B., van Dijken, G. L., D'Ortenzio,
1201 F., and Arrigo, K. R.: Delineating environmental control of phytoplankton biomass and
1202 phenology in the Southern Ocean, *Geophys. Res. Lett.*, 44, 5016–5024, doi:10.1002/
1203 2016GL072428, 2017.

1204 Ardyna, M., Mundy, C. J., Mayot, N., Matthes, L. C., Oziel, L., Horvat, C., Leu, E., Assmy, P.,
1205 Hill, V., Matrai, P. A., Gale, M., Melnikov, I. A., and Arrigo, K. R.: Under-Ice Phytoplankton
1206 Blooms: Shedding Light on the “Invisible” Part of Arctic Primary Production, *Front. Mar. Sci.*,
1207 7, <https://doi.org/10.3389/fmars.2020.608032>, 2020.

1208 Arnscheidt, C. W., Marshall, J., Dutrieux, P., Rye, C. D., and Ramadhan, A.: On the Settling
1209 Depth of Meltwater Escaping from beneath Antarctic Ice Shelves, *JPO*, 51, 2257–2270,
1210 <https://doi.org/10.1175/JPO-D-20-0286.1>, 2021.

1211 Arrigo, K. R., Lowry, K. E., and van Dijken, G. L.: Annual changes in sea ice and phytoplankton
1212 in polynyas of the Amundsen Sea, Antarctica. *Deep-Sea Res. II.*, 71–76, 5–15.
1213 <https://doi.org/10.1016/j.dsr2.2012.03.006>, 2012.

1214 Arrigo, K. R., Robinson, D. H., Worthen, D. L., Dunbar, R. B., DiTullio, G. R., VanWoert, M.,
1215 and Lizotte, M. P.: Phytoplankton community structure and the drawdown of nutrients and CO₂
1216 in the Southern Ocean, *Sci.*, 283, 5400, 365-367, DOI: 10.1126/science.283.5400.365, 1999.

1217

1218 Arrigo, K. R. and van Dijken, G. L.: Phytoplankton dynamics within 37 Antarctic coastal
1219 polynya systems, *J. Geophys. Res. Ocean.*, 108, <https://doi.org/10.1029/2002JC001739>, 2003.

1220 Arrigo, K. R., van Dijken, G. L., and Strong, A. L.: Environmental controls of marine
1221 productivity hot spots around Antarctica, *J. Geophys. Res. Ocean.*, 120, 5545–5565,
1222 <https://doi.org/10.1002/2015JC010888>, 2015.

1223 Arrigo, K. R., Worthen, D., Schnell, A., and Lizotte, M. P.: Primary production in Southern
1224 Ocean waters, *J. Geophys. Res. Ocean.*, 103, 15587–15600, <https://doi.org/10.1029/98JC00930>,
1225 1998.

1226 Assmann, K. M., Jenkins, A., Shoosmith, D. R., Walker, D., Jacobs, S., and Nicholls, K.:
1227 Variability of circumpolar deep water transport onto the Amundsen Sea continental shelf through
1228 a shelf break trough. *J. Geophys. Res. Oceans*, 118, 6603–6620, doi:10.1002/2013JC008871,
1229 2013.

1230 Behrenfeld, M. J. and Falkowski, P. G.: Photosynthetic rates derived from satellite-based
1231 chlorophyll concentration, *Limnol. Oceanogr.*, 42, 1–20,
1232 <https://doi.org/10.4319/lo.1997.42.1.0001>, 1997.

1233 Bett, D. T., Holland, P. R., Naveira Garabato, A. C., Jenkins, A., Dutrieux, P., Kimura, S., and
1234 Fleming, A.: The Impact of the Amundsen Sea Freshwater Balance on Ocean Melting of the
1235 West Antarctic Ice Sheet, *J. Geophys. Res. Oceans*, 125, <https://doi.org/10.1029/2020JC016305>,
1236 2020.

1237 Bhatia, M. P., Kujawinski, E. B., Das, S. B., Breier, C. F., Henderson, P. B., and Charette, M. A.:
1238 Greenland meltwater as a significant and potentially bioavailable source of iron to the ocean,
1239 *Nat. Geosci.*, 6, 274–278, <https://doi.org/10.1038/ngeo1746>, 2013.

1240 Biddle, L. C., Heywood, K. J., Kaiser, J., and Jenkins, A.: Glacial Meltwater Identification in the
1241 Amundsen Sea, *JPO*, 47, 933–954, <https://doi.org/10.1175/JPO-D-16-0221.1>, 2017.

1242 Boles, E., Provost, C., Garçon, V., Bertosio, C., Athanase, M., Koenig, Z., and Sennéchal, N.:
1243 Under-Ice Phytoplankton Blooms in the Central Arctic Ocean: Insights From the First
1244 Biogeochemical IAOOS Platform Drift in 2017, *J. Geophys. Res. Ocean.*, 125, e2019JC015608,
1245 <https://doi.org/10.1029/2019JC015608>, 2020.

1246 Boyd, P. W., Jickells, T., Law, C. S., Blain, S., Boyle, E. A., Buesseler, K. O., Coale, K. H.,
1247 Cullen, J. J., Baar, H. J. W. de, Follows, M., Harvey, M., Lancelot, C., Levasseur, M., Owens, N.
1248 P. J., Pollard, R., Rivkin, R. B., Sarmiento, J., Schoemann, V., Smetacek, V., Takeda, S., Tsuda,
1249 A., Turner, S., and Watson, A. J.: Mesoscale Iron Enrichment Experiments 1993-2005: Synthesis
1250 and Future Directions, *Science*, 315, 612–617, <https://doi.org/10.1126/science.1131669>, 2007.

1251 Cape, M. R., Vernet, M., Pettit, E. C., Wellner, J., Truffer, M., Akie, G., Domack, E., Leventer,
1252 A., Smith, C. R., and Huber, B. A.: Circumpolar Deep Water Impacts Glacial Meltwater Export
1253 and Coastal Biogeochemical Cycling Along the West Antarctic Peninsula, *Front. Mar. Sci.*, 6,
1254 <https://doi.org/10.3389/fmars.2019.00144>, 2019.

1255 Cavalieri, D., Parkinson, C., Gloersen, P., and Zwally, H. J.: Sea Ice Concentrations from
1256 Nimbus-7 SMMR and DMSP SSM/I-SSMIS Passive Microwave Data, Version 1,
1257 <https://doi.org/10.5067/8GQ8LZQVL0VL>, 1996.

1258 Death, R., Wadham, J. L., Monteiro, F., Le Brocq, A. M., Tranter, M., Ridgwell, A., Dutkiewicz,
1259 S., and Raiswell, R.: Antarctic ice sheet fertilises the Southern Ocean, *BG*, 11, 2635–2643,
1260 <https://doi.org/10.5194/bg-11-2635-2014>, 2014.

1261 Dinniman, M. S., St-Laurent, P., Arrigo, K. R., Hofmann, E. E., and Dijken, G. L.: Analysis of
1262 Iron Sources in Antarctic Continental Shelf Waters, *J. Geophys. Res. Oceans.*, 125,
1263 <https://doi.org/10.1029/2019JC015736>, 2020.

1264 Dinniman, M. S., St-Laurent, P., Arrigo, K. R., Hofmann, E. E., and van Dijken, G. L.:
1265 Sensitivity of the Relationship Between Antarctic Ice Shelves and Iron Supply to Projected
1266 Changes in the Atmospheric Forcing, *J. Geophys. Res. Ocean.*, 128, e2022JC019210,
1267 <https://doi.org/10.1029/2022JC019210>, 2023.

1268 Dotto, T. S., Naveira Garabato, A. C., Bacon, S., Holland, P. R., Kimura, S., Firing, Y. L.,
1269 Tsamados, M., Wählén, A. K., and Jenkins, A.: Wind-Driven Processes Controlling Oceanic
1270 Heat Delivery to the Amundsen Sea, Antarctica, *J. Phys. Oceanogr.*, 49, 2829–2849,
1271 <https://doi.org/10.1175/JPO-D-19-0064.1>, 2019.

1272 Douglas, C. C., Briggs, N., Brown, P., MacGilchrist, G., and Naveira Garabato, A.: Exploring
1273 the relationship between sea ice and phytoplankton growth in the Weddell Gyre using satellite
1274 and Argo float data, *Ocean Sci.*, 20, 475–497, <https://doi.org/10.5194/os-20-475-2024>, 2024.

1275 Dutrieux, P., De Rydt, J., Jenkins, A., Holland, P. R., Ha, H., K., Lee, S. H., Steig, E. J., Ding,
1276 Q., Abrahamsen, E. P., and Schröder, M.: Strong sensitivity of Pine Island ice-shelf melting to
1277 climate variability, *Sci.*, 343, 6167, 174–178, DOI: 10.1126/science.1244341, 2014.

1278 ECCO Consortium, Fukumori, I., Wang, O., Fenty, I., Forget, G., Heimbach, P., and Ponte, R.
1279 M: ECCO Ocean Mixed Layer Depth - Monthly Mean 0.5 Degree 9Version 4 Release 4). ver
1280 V4r4. PO.DACC, CA, USA, Dataset accessed [2025-08-22], <https://doi.org/10.5067/ECG5M-OML44>, 2021.

1281 Forsch, K. O., Hahn-Woernle, L., Sherrell, R. M., Rocanova, V. J., Bu, K., Burdige, D., Vernet,
1282 M., and Barbeau, K. A.: Seasonal dispersal of fjord meltwaters as an important source of iron
1283 and manganese to coastal Antarctic phytoplankton, *Biogeo.*, 18, 6349–6375,
1284 <https://doi.org/10.5194/bg-18-6349-2021>, 2021.

1285 Golder, M.R., and Antoine, D.: Physical drivers of long-term chlorophyll-a variability in the
1286 Southern Ocean, *Elem. Sci Anth.*, 13:1, <https://doi.org/10.1525/elementa.2024.00077>, 2025.

1292
1293 Garabato, A. C. N., Forryan, A., Dutrieux, P., Brannigan, L., Biddle, L. C., Heywood, K. J.,
1294 Jenkins, A., Firing, Y. L., and Kimura, S.: Vigorous lateral export of the meltwater outflow from
1295 beneath an Antarctic ice shelf, *Nature*, 542, 219–222, <https://doi.org/10.1038/nature20825>, 2017.

1296 Gerringsa, L. J. A., Alderkamp, A.-C., Laan, P., Thuróczy, C.-E., De Baar, H. J. W., Mills, M. M.,
1297 van Dijken, G. L., Haren, H. van, and Arrigo, K. R.: Iron from melting glaciers fuels the
1298 phytoplankton blooms in Amundsen Sea (Southern Ocean): Iron biogeochemistry, *Deep-Sea*
1299 *Res. II.*, 71–76, 16–31, <https://doi.org/10.1016/j.dsr2.2012.03.007>, 2012.

1300 Gerringsa, L. J. A., Alderkamp, A.-C., Laan, P., Thuróczy, C.-E., de Baar, H. J. W., Mills, M. M.,
1301 van Dijken, G. L., van Haren, H., and Arrigo, K. R.: Corrigendum to “Iron from melting glaciers
1302 fuels the phytoplankton blooms in Amundsen Sea (Southern Ocean): iron biogeochemistry”
1303 (Gerringsa et al., 2012), *Deep-Sea Res. II.*, 177, 104843,
1304 <https://doi.org/10.1016/j.dsr2.2020.104843>, 2020.

1305 Gledhill, M. and Buck, K.: The Organic Complexation of Iron in the Marine Environment: A
1306 Review, *Front. Microbiol.*, 3, <https://doi.org/10.3389/fmicb.2012.00069>. 2012.

1307 Goldberg, D. N., Twelves, A. G., Holland, P. R., & Wearing, K. G.: The non-local impact of
1308 Antarctic subglacial runoff. *Journal of Geophysical Research: Oceans* 128, e2023JC019823.
1309 <https://doi.org/10.1029/2023JC019823>. 2023.

1310 Ha, H. K., Wåhlin, A. K., Kim, T. W., Lee, S. H., Lee, J. H., Lee, H. J., Hong, C. S., Arneborg,
1311 L., Björk, G., and Kalén, O.: Circulation and modification of warm deep water on the central
1312 Amundsen shelf, 44, 5, 1493–1501, <https://doi.org/10.1175/JPO-D-13-0240.1>, 2014.

1313
1314 Hassler, C., Cabanes, D., Blanco-Ameijeiras, S., Sander, S. G., Benner, R., Hassler, C., Cabanes,
1315 D., Blanco-Ameijeiras, S., Sander, S. G., and Benner, R.: Importance of refractory ligands and
1316 their photodegradation for iron oceanic inventories and cycling, *Mar. Fresh. Res.*, 71, 311–320,
1317 <https://doi.org/10.1071/MF19213>, 2019.

1318 Hawkings, J. R., Wadham, J. L., Tranter, M., Raiswell, R., Benning, L. G., Statham, P. J.,
1319 Tedstone, A., Nienow, P., Lee, K., and Telling, J.: Ice sheets as a significant source of highly
1320 reactive nanoparticulate iron to the oceans, *Nat. Commun.*, 5, 3929,
1321 <https://doi.org/10.1038/ncomms4929>, 2014.

1322 Hayward, A., Wright, S. W., Carroll, D., Law, C. S., Wongpan, P., Gutiérrez-Rodríguez, A., and
1323 Pinkerton, M. H.: Antarctic phytoplankton communities restructure under shifting sea-ice
1324 regimes. *Nat. Clim. Chang.* 15, 889–896, <https://doi.org/10.1038/s41558-025-02379-x>, 2025.

1325
1326 Herraiz-Borreguero, L., Lannuzel, D., van der Merwe, P., Treverrow, A., and Pedro, J. B.: Large
1327 flux of iron from the Amery Ice Shelf marine ice to Prydz Bay, East Antarctica, *J. Geophys. Res.*
1328 *Ocean.*, 121, 6009–6020, <https://doi.org/10.1002/2016JC011687>, 2016.

1329 Hersbach, H., Bell, B., Berrisford, P., Hirahara, S., Horányi, A., Muñoz-Sabater, J., Nicolas, J.,
1330 Peubey, C., Radu, R., Schepers, D., Simmons, A., Soci, C., Abdalla, S., Abellán, X., Balsamo,
1331 G., Bechtold, P., Biavati, G., Bidlot, J., Bonavita, M., De Chiara, G., Dahlgren, P., Dee, D.,

1332 Diamantakis, M., Dragani, R., Flemming, J., Forbes, R., Fuentes, M., Geer, A., Haimberger, L.,
1333 Healy, S., Hogan, R. J., Hólm, E., Janisková, M., Keeley, S., Laloyaux, P., Lopez, P., Lupu, C.,
1334 Radnoti, G., de Rosnay, P., Rozum, I., Vamborg, F., Villaume, S., and Thépaut, J.-N.: The ERA5
1335 global reanalysis, *Q. J. R. Meteorol. Soc.*, 146, 1999–2049, <https://doi.org/10.1002/qj.3803>,
1336 2020.

1337 Hosking, J. S., Orr, A., Marshall, G. J., Turner, J., and Phillips, T.: The Influence of the
1338 Amundsen–Bellingshausen Seas Low on the Climate of West Antarctica and Its Representation
1339 in Coupled Climate Model Simulations, *J. Clim.*, 26, 6633–6648, <https://doi.org/10.1175/JCLI-D-12-00813.1>, 2013.

1341 Hosking, J. S., Orr, A., Bracegirdle, T. J., and Turner, J.: Future circulation changes off West
1342 Antarctica: Sensitivity of the Amundsen Sea Low to projected anthropogenic forcing, *Geophys.*
1343 *Res. Lett.*, 43, 367–376, <https://doi.org/10.1002/2015GL067143>, 2016.

1344 Huang, B., Liu, C., Banzon, V., Freeman, E., Graham, G., Hankins, B., Smith, T., and Zhang,
1345 H.-M.: Improvements of the Daily Optimum Interpolation Sea Surface Temperature (DOISST)
1346 Version 2.1, *Journal of Climate*, 34, 2923–2939. doi: 10.1175/JCLI-D-20-0166.1, 2021.

1347 Jacobs, S. S., Jenkins, A., Giulivi, C. F., and Dutrieux, P.: Stronger ocean circulation and
1348 increased melting under Pine Island Glacier ice shelf, *Nat. Geo.*, 4, 519–523,
1349 <https://doi.org/10.1038/ngeo1188>, 2011.

1351 Jena, B. and Pillai, A. N.: Satellite observations of unprecedented phytoplankton blooms in the
1352 Maud Rise polynya, Southern Ocean, *The Cryosphere*, 14, 1385–1398,
1353 <https://doi.org/10.5194/tc-14-1385-2020>, 2020.

1355 Jenkins, A., Dutrieux, P., Jacobs, S. S., McPhail, S. D., Perrett, J. R., Webb, A. T., and White,
1356 D.: Observations beneath Pine Island glacier in West Antarctica and implications for its retreat,
1357 *Nat. Geo.*, 3, 468–472, <https://doi.org/10.1038/NGEO890>, 2010.

1359 Jourdain, N. C., Mathiot, P., Merino, N., Durand, G., Le Sommer, J., Spence, P., Dutrieux, P.,
1360 and Madec, G.: Ocean circulation and sea-ice thinning induced by melting ice shelves in the
1361 Amundsen Sea, *J. Geophys. Res. Ocean.*, 122, 2550–2573,
1362 <https://doi.org/10.1002/2016JC012509>, 2017.

1363 Kauko, H. M., Hattermann, T., Ryan-Keogh, T., Singh, A., de Steur, L., Fransson, A., Chierici,
1364 M., Falkenhaug, T., Hallfredsson, E. H., Bratbak, G., Tsagaraki, T., Berge, T., Zhou, Q., and
1365 Moreau, S.: Phenology and Environmental Control of Phytoplankton Blooms in the Kong Håkon
1366 VII Hav in the Southern Ocean, *Front. Mar. Sci.*, 8, <https://doi.org/10.3389/fmars.2021.623856>,
1367 2021.

1368 Lannuzel, D., Fourquez, M., de Jong, J., Tison, J.-L., Delille, B., and Schoemann, V.: First report
1369 on biological iron uptake in the Antarctic sea-ice environment, *Polar Biol.*, 46, 339–355,
1370 <https://doi.org/10.1007/s00300-023-03127-7>, 2023.

1371 Lee, S. H., Kim, B. K., Lim, Y. J., Joo, H., Kang, J. J., Lee, D., Park, J., Ha, S.-Y., and Lee, S.
1372 H.: Small phytoplankton contribution to the standing stocks and the total primary production in
1373 the Amundsen Sea, BG, 14, 3705–3713, <https://doi.org/10.5194/bg-14-3705-2017>, 2017.

1374 Lee, Y., Park, J., Jung, J., and Kim, T. W.: Unprecedented differences in phytoplankton
1375 community structures in the Amundsen Sea polynyas, West Antarctica, Environ. Res. Lett. 17,
1376 114022, 10.1088/1748-9326/ac9a5f, 2022.

1377 van Leeuwe, M. A., Webb, A. L., Venables, H. J., Visser, R. J. W., Meredith, M., P., Elzenga J.
1379 T. M., and Stefels, J.: Annual patterns in phytoplankton phenology in Antarctic coastal waters
1380 explained by environmental drivers, Limnol. Oceanogr., 65, 1651–1668,
1381 <https://doi.org/10.1002/lno.11477>, 2020.

1382 Liniger, G., Strutton, P. G., Lannuzel, D., and Moreau, S.: Calving event led to changes in
1383 phytoplankton bloom phenology in the Mertz polynya, Antarctica, J. Geophys. Res. Oceans.,
1384 125, e2020JC016387, <https://doi.org/10.1029/2020JC016387>, 2020.

1385 Liu, Y., Moore, J. C., Cheng, X., Gladstone, R. M., Bassis, J. N., Liu, H., Wen, J., and Hui, F.:
1386 Ocean-driven thinning enhances iceberg calving and retreat of Antarctic ice shelves, Proc. Nat.
1387 Acad. Sci., 112, 3263–3268, <https://doi.org/10.1073/pnas.1415137112>, 2015.

1388 van Manen, M., Aoki, S., Brussaard, C. P. D., Conway, T. M., Eich, C., Gerringsa, L., Jung, J.,
1389 Kim, T.-W., Lee, S. H., Lee, Y., Reichart, G.-J., Tian, H., Wille, F., and Middag, R.: The role of
1390 the Dotson Ice Shelf and circumpolar deep water as driver and source of dissolved and
1391 particulate iron and manganese in the Amundsen Sea polynya, Southern Ocean, Mar. Chem.,
1392 104161, <https://doi.org/10.1016/j.marchem.2022.104161>, 2022.

1393 Marchese, C., Albouy, C., Tremblay, J.-É., Dumont, D., D'Ortenzio, F., Vissault, S., and
1394 Bélanger, S.: Changes in phytoplankton bloom phenology over the North Water (NOW)
1395 polynya: a response to changing environmental conditions, Polar Biol., 40, 1721–1737,
<https://doi.org/10.1007/s00300-017-2095-2>, 2017.

1400 Maritorena, S., and Siegel, D. A.: Consistent merging of satellite ocean color data sets using a
1401 bio-optical model, Rem. Sens. Environ., 94, 429–440, <https://doi.org/10.1016/j.rse.2004.08.014>,
1402 2005.

1403 McClish, S., and Bushinsky, S. M.: Majority of Southern Ocean seasonal ice zone bloom net
1404 community production precedes total ice retreat, Geophys. Res. Lett., 50, e2023GL103459.
1405 <https://doi.org/10.1029/2023GL103459>, 2023.

1406 Meredith, M., Sommerkorn, M., Cassotta, S., Derksen, C., Ekaykin, A., Hollowed, A., Kofinas,
1407 G., Mackintosh, A., Melbourne-Thomas, J., Muelbert, M.M.C., Ottersen, G., Pritchard, H., and
1408 Schurr, E.A.G.: Polar Regions. In: *IPCC Special Report on the Ocean and Cryosphere in a
1409 Changing Climate* [H.-O. Pörtner, D.C. Roberts, V. Masson-Delmotte, P. Zhai, M. Tignor, E.
1410 Poloczanska, K. Mintenbeck, A. Alegria, M. Nicolai, A. Okem, J. Petzold, B. Rama, N.M.
1411 Weyer (eds.)]. Cambridge University Press, Cambridge, UK and New York, NY, USA, pp. 203–
1412 320, <https://doi.org/10.1017/9781009157964.005>, 2019.

1413

1414

1415 Mills, M. M., Lindsey, R.K., van Dijken, G. L., Alderkamp, C-A., Berg, G. M., Robinson, D. H.,
1416 Welschmeyer, N. A and Arrigo, K. R.: Photophysiology in two Southern Ocean phytoplankton
1417 taxa: photosynthesis of *phaeocystis antarctica* (prymnesiophyceae) and *fragilioriopsis cylindrus*
1418 (bacillariophyceae) under simulated mixed-layer irradiance, *J. Phycol.*, 46, 1114-1127,
1419 <https://doi.org/10.1111/j.1529-8817.2010.00923.x>, 2010.

1420 Mills, M. M., Alderkamp, C-A., Thuróczy, C-E., van Dijken, G. L., Laan, P., de Barr, H. J. W.
1421 and Arrigo, K. R.: Phytoplankton biomass and pigment responses to Fe amendments on the Pine
1422 Island and Amundsen polynyas, *Deep-Sea Res. II.*, 71-76, 61-76,
1423 <https://doi.org/10.1016/j.dsr2.2012.03.008>, 2012.

1424 Morales Maqueda, M. A.: Polynya Dynamics: a Review of Observations and Modeling, *Rev. Geophys.*, 42, RG1004, <https://doi.org/10.1029/2002RG000116>, 2004.

1426 Moreau, S., Mostajir, B., Bélanger, S., Schloss, I. R., Vancoppenolle, M., Demers, S., and
1427 Ferreyra, G. A.: Climate change enhances primary production in the western Antarctic Peninsula,
1428 *Global Change Biology*, 21, 2191–2205, <https://doi.org/10.1111/gcb.12878>, 2015.

1429 Naughten, K. A., Holland, P. R., and De Rydt, J.: Unavoidable future increase in West Antarctic
1430 ice-shelf melting over the twenty-first century, *Nat. Clim. Change.*, 13, 1222-1228,
1431 <https://doi.org/10.1038/s41558-023-01818-x>, 2023.

1432 Naughten, K. A., Meissner, K. J., Galton-Fenzi, B. K., England, M. H., Timmermann, R., and
1433 Hellmer, H. H.: Future Projections of Antarctic Ice Shelf Melting Based on CMIP5 Scenarios, *J. Clim.*, 31, 5243–5261, <https://doi.org/10.1175/JCLI-D-17-0854.1>, 2018.

1435 Nunes, G.S., Ferreira, A. and Brito, A.C. Long-term satellite data reveals complex phytoplankton
1436 dynamics in the Ross Sea, Antarctica. *Commun. Earth. Environ.*, 6, 864,
1437 <https://doi.org/10.1038/s43247-025-02590-w>, 2025.

1438 Oh, J.-H., Noh, K. M., Lim, H.-G., Jin, E. K., Jun, S.-Y., and Kug, J.-S.: Antarctic meltwater-
1439 induced dynamical changes in phytoplankton in the Southern Ocean, *Environ. Res. Lett.*, 17,
1440 024022, <https://doi.org/10.1088/1748-9326/ac444e>, 2022.

1442 Oliver, H., St-Laurent, P., Sherrell, R. M., and Yager, P. L.: Modeling Iron and Light Controls
1443 on the Summer *Phaeocystis antarctica* Bloom in the Amundsen Sea Polynya, *Global
1444 Biogeochem. Cycles*, 2018GB006168, <https://doi.org/10.1029/2018GB006168>, 2019.

1445 Pan, J. B., Gierach, M. M., Stammerjohn, S., Schofield, O., Meredith, M. P., Reynolds, R. A.,
1446 vernet, M., Haumann, F. A., Orona, A. J., and Miller, C. E.: Impact of glacial meltwater on
1447 phytoplankton biomass along the Western Antarctic Peninsula. *Comm. Earth. Environ.*, 6(456).
1448 <https://doi.org/10.1038/s43247-025-02435-6>. 2025

1449 Paolo, F. S., Fricker, H. A., and Padman, L.: Volume loss from Antarctic ice shelves is
1450 accelerating, *Science*, 348, 327–331, <https://doi.org/10.1126/science.aaa0940>, 2015.

1451 Paolo, F. S., Fricker, H. A., and Padman, L.: Constructing improved decadal records of Antarctic
1452 ice shelf height change from multiple satellite radar altimeters, *Remote Sens. Environ.* 177, 192–
1453 205, <https://doi.org/10.1016/j.rse.2016.01.026>, 2016.

1454 Paolo, F. S., Gardner, A. S., Greene, C. A., Nilsson, J., Schodlok, M. P., Schlegel, N.-J., and
1455 Fricker, H. A.: Widespread slowdown in thinning rates of West Antarctic ice shelves, *TC*, 17,
1456 3409–3433, <https://doi.org/10.5194/tc-17-3409-2023>, 2023.

1457 Park, J., Kuzminov, F. I., Bailleul, B., Yang, E. J., Lee, S., Falkowski, P. G., and Gorbunov, M.
1458 Y.: Light availability rather than Fe controls the magnitude of massive phytoplankton bloom in
1459 the Amundsen Sea polynyas, Antarctica: Light availability rather than Fe controls phytoplankton
1460 bloom, *Limnol. Oceanogr.*, 62, 2260–2276, <https://doi.org/10.1002/lo.10565>, 2017.

1461 Park, J., Kim, J.-H., Kim, H., Hwang, J., Jo, Y.-H., and Lee, S. H.: Environmental Forcings on
1462 the Remotely Sensed Phytoplankton Bloom Phenology in the Central Ross Sea Polynya, *J.*
1463 *Geophys. Res. Ocean.*, 124, 5400–5417, <https://doi.org/10.1029/2019JC015222>, 2019.

1464 Person, R., Aumont, O., Madec, G., Vancoppenolle, M., Bopp, L., and Merino, N.: Sensitivity of
1465 ocean biogeochemistry to the iron supply from the Antarctic Ice Sheet explored with a
1466 biogeochemical model, *BG*, 16, 3583–3603, <https://doi.org/10.5194/bg-16-3583-2019>, 2019.

1467 Pritchard, H. D., Ligtenberg, S. R. M., Fricker, H. A., Vaughan, D. G., van den Broeke, M. R.,
1468 and Padman, L.: Antarctic ice-sheet loss driven by basal melting of ice shelves, *Nat.*, 484, 502–
1469 505, <https://doi.org/10.1038/nature10968>, 2012.

1470 Racault, M.-F., Le Quéré, C., Buitenhuis, E., Sathyendranath, S., and Platt, T.: Phytoplankton
1471 phenology in the global ocean, *Ecol. Indic.*, 14, 152–163,
1472 <https://doi.org/10.1016/j.ecolind.2011.07.010>, 2012.

1473 Randall-Goodwin, E., Meredith, M. P., Jenkins, A., Yager, P. L., Sherrell, R. M., Abrahamsen,
1474 E. P., Guerrero, R., Yuan, X., Mortlock, R. A., Gavahan, K., Alderkamp, A.-C., Ducklow, H.,
1475 Robertson, R., and Stammerjohn, S. E.: Freshwater distributions and water mass structure in the
1476 Amundsen Sea Polynya region, Antarctica, *Elem. Sci. Anth.*, 3, 000065,
1477 <https://doi.org/10.12952/journal.elementa.000065>, 2015.

1478 Rignot, E., Jacobs, S., Mouginot, J., and Scheuchl, B.: Ice-Shelf Melting Around Antarctica, *Sci.*,
1479 341, 266–270, <https://doi.org/10.1126/science.1235798>, 2013.

1480 Rignot, E., Mouginot, J., Scheuchl, B., van den Broeke, M., van Wessem, M. J., and Morlighem,
1481 M.: Four decades of Antarctic Ice Sheet mass balance from 1979–2017, *Proc. Nat. Acad. Sci.*,
1482 116, 4, 1095–1103, <https://doi.org/10.1073/pnas.1812883116>, 2019.

1483 Ryan-Keogh, T. J., Thomalla, S. J., Chang, N., and Moalusi, T.: A new global oceanic multi-
1484 model net primary productivity data product, *Earth Syst. Sci. Data*, 15, 4829–4848,
1485 <https://doi.org/10.5194/essd-15-4829-2023>, 2023.

1486
1487 Sari El Dine, Z., Guinet, C., Picard, B., Thyssen, M., Duforêt-gaurier, L., and El Hourany,
1488 R.: Influence of the phytoplankton community structure on the southern elephant seals' foraging

1489 activity within the Southern Ocean, *Commun. Biol.*, 8, 620, <https://doi.org/10.1038/s42003-025-08049-0>, 2025.

1490

1491

1492 Scambos, T., Bell, R. E., Alley, R. B., Anandakrishnan, S., Bromwich, D. H., Brunt, K.,

1493 Christianson, K., Creyts, T., Das, S. B., DeConto, R., Dutrieux, P., Fricker, H. A., Holland, D.,

1494 MacGregor, J., Medley, B., Nicolas, J. P., Pollard, D., Siegfried, M. R., Smith, A. M., Steig, E.

1495 J., Trusel, L. D., Vaughan, D. G., and Yager, P. L.: How much, how fast?: A science review and

1496 outlook for research on the instability of Antarctica's Thwaites Glacier in the 21st century, *Glob.*

1497 *Planet. Change.*, 153, 16-34, <https://doi.org/10.1016/j.gloplacha.2017.04.008>, 2017.

1498

1499 Silsbe, G. M., Behrenfeld, M. J., Halsey, K. H., Milligan, A. J., and Westberry, T. K.: The CAFE

1500 model: A net production model for global ocean phytoplankton, *Global Biogeochem. Cycles.*,

1501 30, 1756–1777, doi:10.1002/2016GB005521, 2016.

1502 Shepherd, A., Ivins, E., Rignot, E., Smith, B., van den Broeke, M., Velicogna, I., Whitehouse, P.,

1503 Briggs, K., Joughin, I., Krinner, G., Nowicki, S., Payne, T., Scambos, T., Schlegel, N., A. G.,

1504 Agosta, C., Ahlstrøm, A., Babonis, G., Barletta, V., Blazquez, A., Bonin, J., Csatho, B.,

1505 Cullather, R., Felikson, D., Fettweis, X., Forsberg, R., Gallee, H., Gardner, A., Gilbert, L., Groh,

1506 A., Gunter, B., Hanna, E., Harig, C., Helm, V., Horvath, A., Horwath, M., Khan, S., Kjeldsen, K.

1507 K., Konrad, H., Langen, P., Lecavalier, B., Loomis, B., Luthcke, S., McMillan, M., Melini, D.,

1508 Mernild, S., Mohajerani, Y., Moore, P., Mouginot, J., Moyano, G., Muir, A., Nagler, T., Nield,

1509 G., Nilsson, J., Noel, B., Otosaka, I., Pattle, M. E., Peltier, W. R., Pie, N., Rietbroek, R., Rott, H.,

1510 Sandberg-Sørensen, L., Sasgen, I., Save, H., Scheuchl, B., Schrama, E., Schröder, L., Seo, K.-

1511 W., Simonsen, S., Slater, T., Spada, G., Sutterley, T., Talpe, M., Tarasov, L., van de Berg, W. J.,

1512 van der Wal, W., van Wessem, M., Vishwakarma, B. D., Wiese, D., Wouters, B., and The

1513 IMBIE team: Mass balance of the Antarctic Ice Sheet from 1992 to 2017, *Nat.*, 558, 219–222,

1514 <https://doi.org/10.1038/s41586-018-0179-y>, 2018.

1515 Sherrell, R. M., Lagerström, M. E., Forsch, K. O., Stammerjohn, S. E., and Yager, P. L.:

1516 Dynamics of dissolved iron and other bioactive trace metals (Mn, Ni, Cu, Zn) in the Amundsen

1517 Sea Polynya, Antarctica, *Elementa: Sci. Anthropol.*, 3, 000071,

1518 <https://doi.org/10.12952/journal.elementa.000071>, 2015.

1519 Siegel, D. A., Doney, S. C., and Yoder, J. A.: The North Atlantic Spring Phytoplankton Bloom

1520 and Sverdrup's Critical Depth Hypothesis, *Science*, 296, 730–733,

1521 <https://doi.org/10.1126/science.1069174>, 2002.

1522 Smith, A. J. R., Nelson, T., Ratnarajah, L., Genovese, C., Westwood, K., Holmes, T. M., Corkill,

1523 M., Townsend, A. T., Bell, E., Wuttig, K., and Lannuzel, D.: Identifying potential sources of

1524 iron-binding ligands in coastal Antarctic environments and the wider Southern Ocean, *Front.*

1525 Mar. Sci.

1526 Soppa, M. A., Völker, C., and Bracher, A.: Diatom Phenology in the Southern Ocean: Mean

1527 Patterns, Trends and the Role of Climate Oscillations, *Remote Sens.*, 8, 420,

1528 <https://doi.org/10.3390/rs8050420>, 2016.

1529 Stammerjohn, S. E., Martinson, D. G., Smith, R. C., and Iannuzzi, R. A.: Sea ice in the western
1530 Antarctic Peninsula region: Spatio-temporal variability from ecological and climate change
1531 perspectives, *Deep-Sea Res. II.*, 55, 2041–2058, <https://doi.org/10.1016/j.dsr2.2008.04.026>,
1532 2008.

1533 Stoer, A. C., and Fennel, K.: Carbon-centric dynamics of Earth's marine phytoplankton, *Proc.
1534 Nat. Acad. Sci.*, 121, 45, e2405354121, <https://doi.org/10.1073/pnas.2405354121>
1535 , 2024.

1536

1537 St-Laurent, P., Yager, P. L., Sherrell, R. M., Stammerjohn, S. E., and Dinniman, M. S.: Pathways
1538 and supply of dissolved iron in the Amundsen Sea (Antarctica), *J. Geophys. Res. Oceans.*, 122,
1539 7135–7162, <https://doi.org/10.1002/2017JC013162>, 2017.

1540 St-Laurent, P., Yager, P. L., Sherrell, R. M., Oliver, H., Dinniman, M. S., and Stammerjohn, S.
1541 E.: Modeling the Seasonal Cycle of Iron and Carbon Fluxes in the Amundsen Sea Polynya,
1542 Antarctica, *J. Geophys. Res. Oceans.*, 124, 1544–1565, <https://doi.org/10.1029/2018JC014773>,
1543 2019.

1544 Tagliabue, A., Bowie, A. R., DeVries, T., Ellwood, M. J., Landing, W. M., Milne, A., Ohnemus,
1545 D. C., Twining, B. S., and Boyd, P. W.: The interplay between regeneration and scavenging
1546 fluxes drives ocean iron cycling, *Nat Commun.*, 10, 4960, [https://doi.org/10.1038/s41467-019-12775-5](https://doi.org/10.1038/s41467-019-
1547 12775-5), 2019.

1548 Tamsitt, V., England, M. H., Rintoul, S. R., and Morrison, A. K.: Residence Time and
1549 Transformation of Warm Circumpolar Deep Water on the Antarctic Continental Shelf, *Geophys.
1550 Res. Lett.*, 48, e2021GL096092, <https://doi.org/10.1029/2021GL096092>, 2021.

1551 Tamura, T. P., Nomura, D., Hirano, D., Tamura, T., Kiuchi, M., Hashida, G., Makabe, R., Ono,
1552 K., Ushio, S., Yamazaki, K., Nakayama, Y., Takahashi, K. D., Sasaki, H., Murase, H., and Aoki,
1553 S.: Impacts of basal melting of the Totten Ice Shelf and biological productivity on marine
1554 biogeochemical components in Sabrina Coast, East Antarctica, *Global Biogeochem. Cycles.*, 37,
1555 e2022GB007510, <https://doi.org/10.1029/2022GB007510>, 2023.

1556 Thomalla, S.J., Nicholson, S.A., Ryan-Keogh, T.J. *et al.* Widespread changes in Southern Ocean
1557 phytoplankton blooms linked to climate drivers. *Nat. Clim. Chang.* 13, 975–984,
1558 <https://doi.org/10.1038/s41558-023-01768-4>, 2023.

1559 Thuróczy, C.-E., Alderkamp, A.-C., Laan, P., Gerringa, L. J. A., Mills, M. M., van Dijken, G. L.,
1560 De Baar, H. J. W., and Arrigo, K. R.: Key role of organic complexation of iron in sustaining
1561 phytoplankton blooms in the Pine Island and Amundsen Polynyas (Southern Ocean), *Deep-Sea
1562 Res. II.*, 71–76, 49–60, <https://doi.org/10.1016/j.dsr2.2012.03.009>, 2012.

1563 Turner, J., Hosking, J. S., Marshall, G. J., Phillips, T., and Bracegirdle, T. J.: Antarctic sea ice
1564 increase consistent with intrinsic variability of the Amundsen Sea Low, *Clim. Dyn.*, 46, 2391–
1565 2402, <https://doi.org/10.1007/s00382-015-2708-9>, 2016.

1566 [Twelves, A. G., Goldberg, D. N., Henley, S. F., Mazloff, M. R. and Jones, D. C.: Self-shading
1567 and meltwater spreading control the transition from light to iron limitation in an Antarctic coastal](#)

1568 polynya. *J. Geophys. Res. Oceans.*, 126, e2020JC016636,
1569 [https://doi.org/10.1029/2020JC016636, 2021.](https://doi.org/10.1029/2020JC016636)
1570

1571 Vaillancourt, R. D., Sambrotto, R. N., Green, S., and Matsuda, A.: Phytoplankton biomass and
1572 photosynthetic competency in the summertime Mertz Glacier Region of East Antarctica, Deep-
1573 Sea Res. II., 50, 1415–1440, [https://doi.org/10.1016/S0967-0645\(03\)00077-8](https://doi.org/10.1016/S0967-0645(03)00077-8), 2003.

1574 Westberry, T., Behrenfeld, M. J., Siegel, D. A., and Boss, E.: Carbon-based primary productivity
1575 modeling with vertically resolved photoacclimation, *Global Biogeoch. Cycle.*, 22, GB2024,
1576 doi:10.1029/2007GB003078, 2008.

1577

1578 Yager, P. L., Sherrell, R. M., Stammerjohn, S., Alderkamp, A.-C., Schofield, O., Abrahamsen, P.,
1579 Arrigo, K., Bertilsson, S., Garay, L., Guerrero, R., Lowry, K., Moksnes, P.-O., Ndungo, K., Post,
1580 A., Randall-Goodwin, E., Riemann, L., Severmann, S., Thatje, S., van Dijken, G., and Wilson,
1581 S.: ASPIRE: The Amundsen Sea Polynya International Research Expedition, *Oceanog.*, 25, 40–
1582 53, <https://doi.org/10.5670/oceanog.2012.73>, 2012.

1583 Yager P. L, Sherrell, R.M., Stammerjohn, S.E., Ducklow, H. W., Schofield, O., Ingall E.D.,
1584 Wilson, S. E., Lowry, K. E., Willismd, C. M., Riemman, L., Bertilsson, S., Alderkamp, A-C.,
1585 Dinasquet, J., Logares, R., Richert, I., Sipler, R. E., Melara A. J., Mu, L., Newstead, R. G., Post,
1586 A. F., Swalethorp, R and van Dijken, G. L.: A carbon budget for the Amundsen Sea Polynya,
1587 Antarctica: Estimating net community production and export in a highly productive polar
1588 ecosystem, *Elem. Sci. Anth.*, 4, 000140, doi: 10.12952/journal.elementa.000140, 2016.

1589 Yu, L.-S., He, H., Leng, H., Liu, H., and Lin, P.: Interannual variation of summer sea surface
1590 temperature in the Amundsen Sea, Antarctica, *Front. Mar. Sci.*, 10,
1591 <https://doi.org/10.3389/fmars.2023.1050955>, 2023.

1592 Zheng, Y., Heywood, K. J., Webber, B. G. M., Stevens, D. P., Biddle, L. C., Boehme, L., and
1593 Loose, B.: Winter seal-based observations reveal glacial meltwater surfacing in the southeastern
1594 Amundsen Sea, *Commun. Earth. Environ.*, 2, 1–9, <https://doi.org/10.1038/s43247-021-00111-z>,
1595 2021.

1596

Page 11: [1] Deleted	Author	1/8/26 10:40:00 AM
Page 12: [2] Deleted	Author	1/8/26 10:40:00 AM
Page 19: [3] Deleted	Author	1/8/26 10:40:00 AM